DYNATECH R/D COMPANY

THERMAL ENERGY STORAGE MATERIAL THERMOPHYSICAL PROPERTY MEASUREMENT AND HEAT TRANSFER IMPACT

Prepared by:

R. P. Tye

J. G. Bourne

A. O. Desjarlais

Prepared for:

National Aeronautics and Space Administration
Lewis Research Center
Cleveland, Ohio

Dynatech Report No. 1503

Work carried out under Contract No. NAS-3-19716

NASA Report No. NASA-CR-135098

August 11, 1976

a division of DYNATECH CORPORATION

THERMAL ENERGY STORAGE MATERIAL THERMOPHYSICAL PROPERTY MEASUREMENT AND HEAT TRANSFER IMPACT

Prepared by:

R. P. Tye

J. G. Bourne

A. O. Desjarlais

Prepared for:

National Aeronautics and Space Administration
Lewis Research Center
Cleveland, Ohio

Dynatech Report No. 1503

Work carried out under Contract No. NAS-3-19716

NASA Report No. NASA-CR-135098

August 11, 1976

DYNATECH R/D COMPANY
A Division of Dynatech Corporation
99 Erie Street
Cambridge, Massachusetts 02139

Telephone: (617) 868-8050

TABLE OF CONTENTS

TABLE OF CONTENTS (Concluded)

LIST OF FIGURES

LIST OF TABLES

NOMENCLATURE

A	Area, m^2
C_p	Specific heat, J/kgK
h_F	Heat of fusion, J/kg
Q	Thermal energy, J
q	Heat flow, W
r	Radius, m
t	Time, s
T	Temperature, K
T_m	Melt temperature, K
T_s	Solid temperature, K
x	Distance, m
V	Volume, m^3
ρ	Density, kg/m^3
ρ_ℓ	Liquid density, kg/m^3
ρ_s	Solid density, kg/m^3
λ	Thermal conductivity, W/mK
Δ	Thickness, m

Section 1

SUMMARY

The work described in this report was carried out at Dynatech R/D Company for the National Aeronautics and Space Administration Lewis Research Center under Contract NAS-3-19716 with Mr. J. P. Joyce as the technical monitor.

The major purpose of the investigation was to select and measure the thermophysical properties of salts having potential for thermal energy storage to provide peaking energy in conventional electric utility power plants.

Four candidate classes of electric power plants were considered. The systems and the selected salt for each were:

1. Pressurized Water Reactor } - $LiNO_3$ m.p. ~ 527K
2. Boiling Water Reactor } - 63 LiOH/37 LiCl eutectic m.p. ~ 533K
3. Supercritical Steam Reactor - LiOH m.p. ~ 743K
4. High Temperature Gas Reactor - $Na_2B_4O_7$ m.p. ~ 1015K

The thermal conductivity, specific heat (including latent heat of fusion), and density of each salt were measured for a temperature range of at least $\pm$ 100K of the measured melt point. Measurements were made with both reagent and commercial grades of each salt. Where necessary techniques were developed to fabricate and prepare uncontaminated, close-to-theoretical-density solid samples for the measurements. The results are presented and discussed, in relation both to the very limited data available for any of the materials and to their potential use as thermal energy storage salts. Little difference in any property was found between the reagent and commercial grades of any of the four materials.

The lithium salts are good candidate materials since they have relatively high specific heats and high latent heats of fusion (of the order

of 5 - 10 x 10^5 J/kg). However, heat transfer is poor by reason of the typically low values of thermal conductivity (of the order of 1 W/mK). The thermal conductivity of the solid decreases with increase in temperature and there is an approximate 50% decrease at the melting point, followed by a small increase with increase of temperature. The density of the two lower temperature materials decreases at the melting point by over 20%. The lithium hydroxide decreases by only 2%.

Sodium diborate is a poor energy storage material since it does not appear to have a very high latent heat and has an apparent increase in density on melting. It behaves in an anomalous manner in the 500 to 700C regime, due presumably to the formation of a supercooled amorphous form.

Following the measurements, a storage system was sized for association with a boiling water reactor of the class of the Braun SAR. The design conditions for the system were:

Design Power	1250 MW
Peaking Power	250 MW
Storage Capacity (Electric)	600 MW-hr

From the results of the measurements $LiNO_3$ was preferred to the eutectic for this application.

The design of this storage system required the following:

Total mass of heat of storage material	19.2 x 10^6 kg
Total volume of tank to contain heat	11600 m^3
Total length of 0.025 m stainless steel tubing	1.7 x 10^6 m

Section 2

SELECTION OF HEAT STORAGE MATERIALS

2.1 Concept of Storage System

2.1.1 Power System Load

Typically, electric power networks have a variable annual load demand, as shown in Figure 2.1 (Ref. 1). When the nature of this demand is such that excess base load generating capacity is available, energy storage systems, which can level some of the peaks and valleys of the time-variable load, become attractive. By more effectively using the most efficient generating equipment, energy storage systems can meet overall network electrical requirements while reducing the cost of producing electricity and, possibly, the total energy input.

Generating stations in an electric power network are classified as base load, intermediate cycling, or peaking, in accordance with the number of hours per year they are in operation. Base load plants are designed to be operated continuously throughout the year. In order to minimize their operating cost, base load plants are highly efficient, but relatively inflexible from the standpoint of power output. Intermediate cycling plants provide for daily cyclic loading, are generally somewhat less efficient and more costly to operate, and are brought on line between eight and twelve hours per day, or approximately 3000 hours per year. Peaking plants are used only during periods of peak demand, are generally costly to operate, and are operated less than 1000 hours per year.

2.1.2 Energy Storage

Energy storage has been applied by electric utilities on a system basis for a number of years. Initially, when hydraulic power was an important component of the available system power, run of river storage was used to handle a large portion of the variable demand. This method was very effective, since

Figure 2.1

Typical Weekly Load Duration Curve

Northeast Regional System

Circa 1990

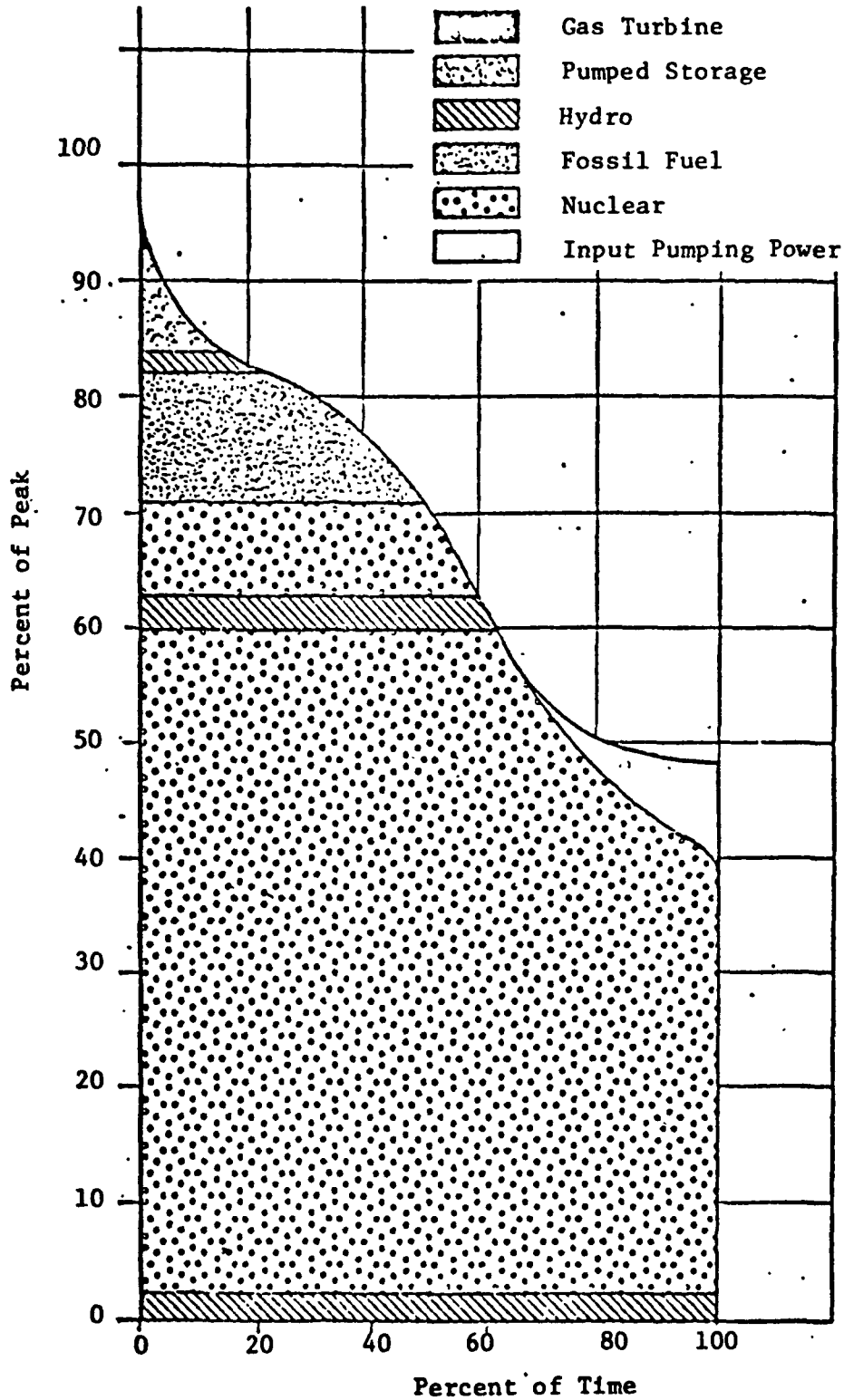

the initial cost of the facility was primarily in the dam and the efficiency of power production was relatively independent of rate.

Pumped water storage is the principal method implemented in American electric utilities. Water is pumped into a reservoir during periods of low demand, or when available electric power is economically priced, and drawn out through a power turbine to provide peak loads. Pumped storage does introduce an inefficiency in the product of the component efficiencies of the pump and the turbine, normally between fifty and seventy percent. The total capacity available from this class of storage is limited by the natural sites available.

A pumped storage unit is a separate component of the utility system. It receives and provides power to the electric network as a whole. Hence, its overall operating efficiency and cost should be penalized by the inefficiencies and costs of operating the electric network.

2.1.3 High Temperature Thermal Storage

High temperature thermal storage, the alternate technique under consideration in this study, receives energy in the form of heat rather than electricity. Therefore, it is intimately related to a specific power plant.

Thermal storage receives excess heat generated in a relatively efficient unit and gives this energy to a power conversion system during periods of peak demand. Because of their high efficiency and low flexibility, base load plants with periodic excess capacity are ideal locations for high temperature thermal storage systems. To the extent that excess capacity exists in base load plants in a network, thermal energy storage systems can augment or replace less efficient, more costly peaking equipment.

Thermal storage could be applied to a cycling power plant. On a twelve hour cycling plant, heat would go into storage half the time and be drawn from storage and the heat generator during the other half. The power producer in this case would be twice the size of the power producer for a base load power plant using the same heat source.

The design conditions for this case are specified by the project monitor for a peaking application (Reference 2). These recommendations are given in Table 2.1.

Table 2.1

STORAGE SYSTEM DESIGN SPECIFICATIONS

	Absolute	% of Daily Base Load
Base Load Plant, MW_e	1000	100%
Peaking Power Rate, MW_e	200	20%
Storage Capacity, MW_e-hr (Electric)	480	2%

The two percent of equivalent electric output to storage requires more than two percent of the heat input. If the storage is being filled continually by an increased production of thermal energy by the heat source, this increase amounts to about three percent of plant design capacity (two percent divided by the estimated efficiency of the overall peaking system relative to the base load plant). If the storage is being filled during five hours of reduced demand, the reduction in plant output is twenty to thirty percent. The heat input to the cycle is reduced by 15% as the storage unit is building up its ability to produce electric power at the rate of 10% of base load capacity. In addition, there is a reduction in the cycle efficiency at part load.

2.1.4 Classes of Storage Materials

High temperature thermal storage can use either sensible heat or heat of fusion as an energy receiver. Heat of fusion has the advantage of permitting a relatively small receiver design, since a large amount of energy can be stored per unit volume of the storage material. It has the disadvantage, as compared to a liquid storage medium, of requiring heat transfer through a solid which is likely to be a poor conductor. In this contract we are considering only heat of fusion materials.

Candidate materials include pure substances and eutectic mixtures which solidify at a constant temperature. This permits design at a maximum effective temperature difference between the source temperature and the temperature at which the peaking power system receives heat, as shown in Figure 2.2. Non-eutectic mixtures may have a narrow melting temperature which would not affect the temperature difference appreciably. However, during melting and solidification there is a gradual segregation of the mixture components, since the equilibrium mixture ratios are not equal at the solid-liquid interface. One component is preferentially depleted from the solid, and the characteristics change over time. Thus non-eutectic mixtures are not desirable.

2.2 Factors Affecting Storage Material Selection

High temperature thermal storage is a component of a system to provide peaking power for an electric utility network. The ultimate decision on the application of this concept is economic, based on the total cost of such a system as compared to a comparable peaking plant to satisfy the same region of the power spectrum, and is conservative, based on possible savings in oil and gas typically used in peaking plants. The final selection of the material is dependent upon its effect on the cost of the storage component. In the process of material selection, without a specific design under consideration, it is only possible to determine the trends of this effect, in terms of relative values for different candidate substances.

The three components of the thermal storage system are: the heat transfer component that transfers heat from the prime source, the heat transfer component that transfers heat to the power cycle, and the storage vessel that contains the heat storage material. The precise relationship between the cost of these components depends upon the method of design integration. However, the cost of the two heat transfer units generally is proportional to heat transfer area, and the cost of the storage vessel is an increasing function of total volume. The cost of the storage material is directly proportional to the required volume.

Figure 2.2

Temperature Range of Storage System

Boiling Water Reactor

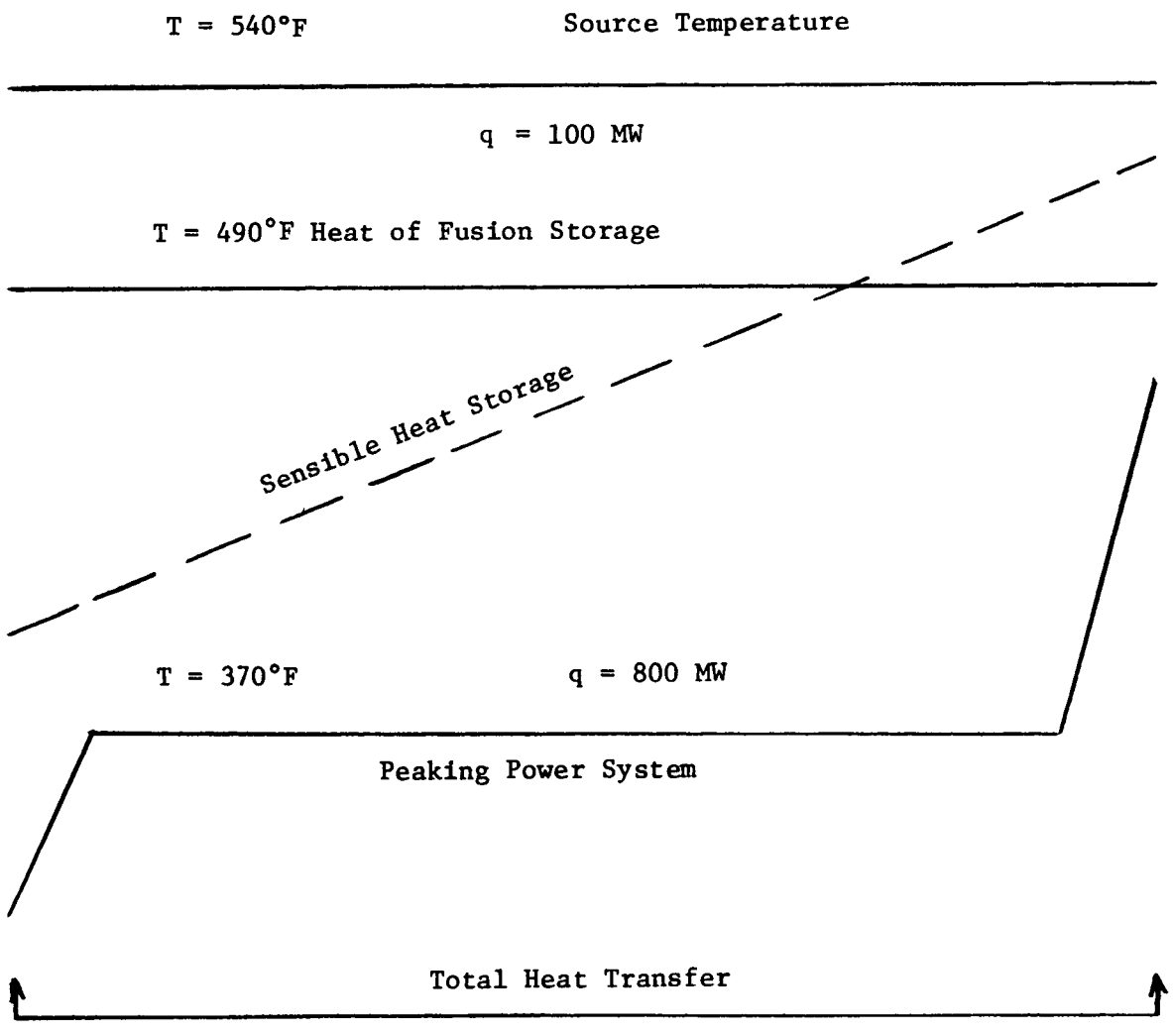

The principal property of the storage material which determines the heat transfer area is the thermal conductivity of the solid. Heat is transferred from a flowing cycle fluid through the vessel, through a solid layer of the storage material, to the solid-liquid interface. The same process occurs in reverse when the heat is supplied to the peaking cycle. Therefore, heat has to be transferred through an accumulating or decreasing layer of solid. To the extent that this layer controls the heat transfer, the desirable heat transfer parameter is $(\lambda h_F \rho)^{1/2}$ (see Appendix A). If the storage vessel is separate, the cost of the containment vessel is a function of a volume parameter, $h_F \rho$. If the heat transfer surface acts as the outside wall of the storage vessel, the total cost of material required determines the storage cost parameter. This is proportional to h_F/C.

Other properties also affect cost. Corrosiveness of the salt determines the compatible materials and thus the costs. The expansion during melting determines the necessary expansion provisions to be incorporated into the design. The specific heat may affect the useful enthalpy change during melting if a wide temperature range is used.

With the limited selection of materials in the proper temperature ranges, and limited data availability on thermal conductivity, the cost parameter and the volume parameter are used for selection. Excessive corrosiveness is cause for elimination, as is lack of availability in large quantities.

2.3 Systems to be Considered

Four classes of power plants are candidates for high temperature thermal storage systems. These are:

1. Boiling water nuclear reactors.
2. Pressurized water nuclear reactors.
3. Supercritical, fossil fuel fired, steam systems.
4. High temperature gas reactors.

This selection of candidates leads to three temperature ranges of interest. These are:

Water-cooled reactors	910 - 980R
Super critical steam	1410 - 1535R
Gas cooled reactors	1760 - 1860R

Their thermodynamic cycles determine the appropriate temperature range for the given application.

The precise temperature range depends upon the cycle configuration. Figure 2.3 shows two potential overall configurations: one with the storage system in parallel; the other, in series. From the standpoint of the power plant, it is desirable to have the storage system in parallel because it minimizes the effect on the power plant system. From the standpoint of the storage system, it is better to have the series arrangement if there is an appreciable temperature drop in cycle working fluid. (A series arrangement with the storage unit following the power system puts a maximum penalty on the storage system.) Table 2.2 gives the minimum temperature of the fluid supplied to the storage system for each mode of operation described above. Since the water cooled reactors supply heat over a small temperature range, the mode of operation has little effect on the design temperature. For the higher temperature systems, parallel operation severely limits the temperature range of operation.

The pressurized water reactor and the boiling water reactor have virtually the same temperature requirements. Two materials are selected, either of which may prove to be superior when more definitive information about properties is available.

Figure 2.3

Cycle Configurations

Pressurized Water Reactor

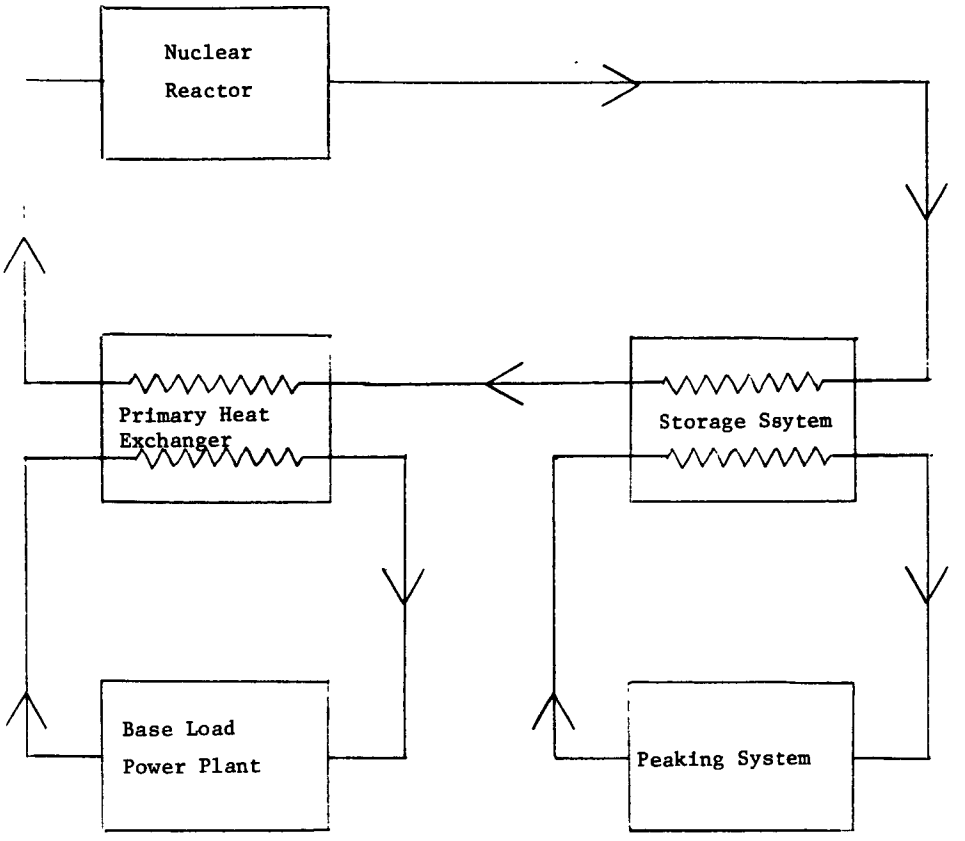

Series

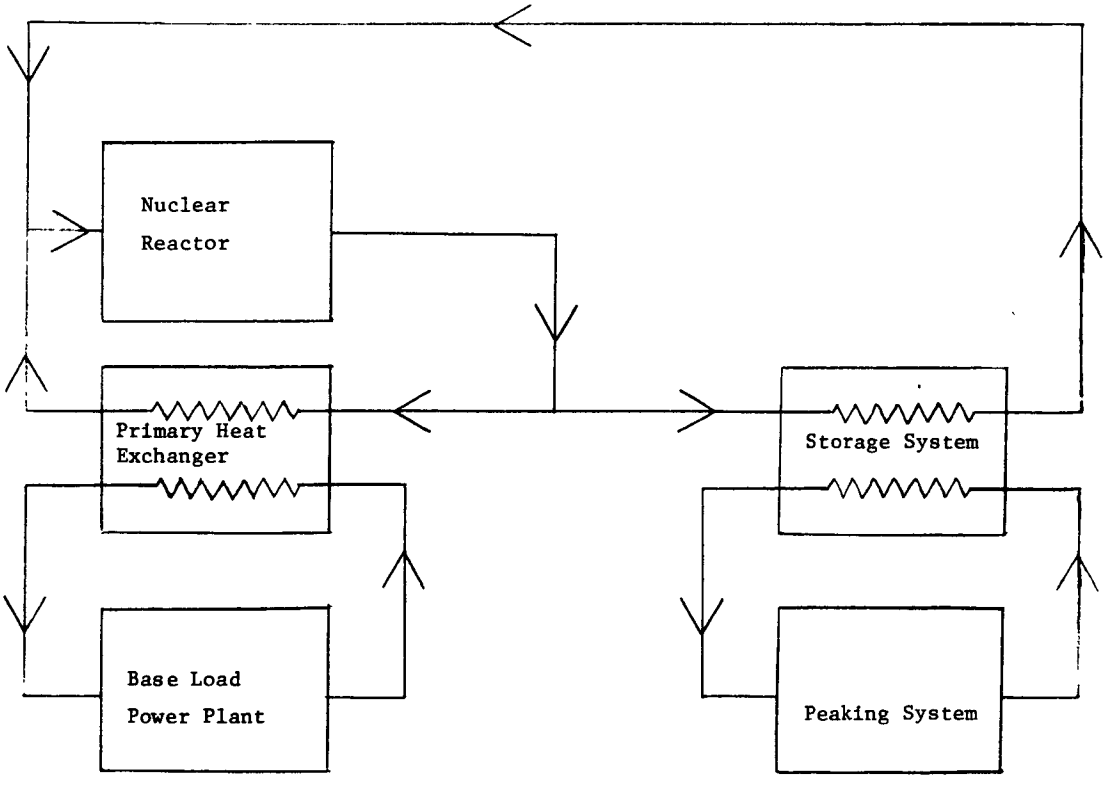

Parallel

Table 2.2

STORAGE DESIGN TEMPERATURE RANGE FOR SPECIFIC POWER PLANTS

		Boiling Water Reactor	Pressurized Water Reactor	Supercritical Steam	High Temperature Gas Reactor
Contractual Temperature Range °K	High	539	544	853	1033
	Low	506	511	783	978
Temperature Range of Working Fluid °K	High	559	591	811	1040
	Low	551	563	551	603
Minimum Temperature Available to Storage for Several Cycle Configurations	Series, Constant Heat Removal	559	590	803	1027
	Series, Nighttime Heat Removal	558	587	772	974
	Parallel	551	563	551	603

2.4 Comparison of Potential Heat Storage Materials

2.4.1 Materials Under Consideration

A review is made of all potential heat of fusion materials over the range of temperatures from 450 K to 1150 K. Table 2.3 lists these materials, the corresponding melt temperatures, estimated heats of fusion, and densities. This list exceeds the potential operating ranges of the cycles under consideration and is not limited to the temperature range for the specific cycles. This is a reference list given for future application of heat storage materials at other temperatures. Materials omitted from this list are not considered.

Table 2.4 gives additional properties, where available, for the materials in Table 2.3. Since there is only a limited amount of thermal conductivity data available, it is difficult to apply the heat transfer parameter for comparison. Thus only the volumetric heat of fusion, which is a factor in this parameter, is used.

2.4.2 Selection of Materials for Water Cooled Reactors

Table 2.5 lists the candidate materials in the specified temperature range and gives the effective latent heat on a cost and volume basis. Sodium hydroxide has too high a melt temperature, and the next three candidates are marginal in melt temperature, being incompatible with the boiling water reactor. All materials are available in car load lots, and none of the materials exhibit major compatibility problems.

$NaNO_3$-NaCl among the three marginal candidates is eliminated because its volumetric heat of fusion is low. The other two are comparable, both on a cost and volume basis.

LiOH-NaOH is eliminated because it has a low volumetric latent heat, a low temperature of fusion, and a high relative cost. Both $LiNO_3$ and LiCl-LiOH are expensive, but they have good volumetric heat of fusion properties,

Table 2.3

HIGH TEMPERATURE HEAT OF FUSION MATERIALS

No.	Material	Melt Temp. °K	Heat of Fusion kJ/kg	Density kg/m^3
1	KF	1125	454	2480
2	Na_2CO_3	1125	279	2530
3	Ca	1123	221	1540
4	LiF	1121	1044	2640
5	$LiBO_2$	1108	698	1400
6	75 NaF + 25 MgF_2	1105	649	2680
7	62.5 NaF + 22.5 MgF_2 + 15 KF	1082	607	2630
8	NaCl	1074	484	2180
9	CaI_2	1057	142	3490
10	$CaCl_2$	1046	256	2280
11	KCl	1043	372	1990
12	67 LiF + 33 MgF_2	1019	947	2630
13	65 NaF + 23 CaF_2 + 23 MgF_2	1018	574	2760
14	$Na_2B_4O_7$	1013	523	2370
15	Li_2CO_3	998	605	2200
16	$MgCl_2$	988	454	2240
17	60 KF + 40 NaF	983	479	2510
18	LiH	956	2582	790
19	Al	933	388	2710
20	60 LiF + 40 NaF	925	816	2480
21	Mg	923	372	1740
22	46 LiF + 44 NaF + 10 MgF_2	905	858	2610
23	52 LiF + 35 NaF + 13 CaF_2	888	640	2630
24	LiCl	883	470	2070
25	52 NaCl + 48 $NiCl_2$	843	558	2840
26	$Ca(NO_3)_2$	834	130	2500
27	73 LiCl + 27 NaCl	825	430	2090
28	48 NaCl + 52 $CaCl_2$	773	328	2160
29	49 KF + 51 LiF	765	461	2560
30	80 Li_2CO_3 + 20 K_2CO_3	763	377	2170
31	LiOH	743	930	1460
32	11.5 NaF + 42 KF + 46.5 LiF	727	442	2560
33	NaCl + $MgCl_2$	713	326	2240
34	80 LiOH + 20 LiF	700	1163	1550
35	KOH	673	140	2040
36	LiCl + KCl	623	255	2030
37	KNO_3	613	128	2110
38	NaOH	593	160	2070
39	$Na_2N_2O_2$	588	244	1730
40	93.6 $NaNO_3$ + 6.4 NaCl	568	191	2260
41	95.3 NaOH + 4.7 Na_2SO_4	566	326	-
42	7.8 NaCl + 6.4 Na_2CO_3 + 85.8 NaOH	555	316	2100
43	37 LiCl + 63 LiOH	535	437	1640
44	NaCl + $ZnCl_2$	533	198	2480
45	23 LiOH + 77 NaOH	528	233	1890
46	$LiNO_3$	527	379	2400
47	$AlCl_3$	468	290	2440
48	NaOH + KOH	463	233	2060
49	Li	453	442	530

Table 2.4

AVAILABLE THERMAL PROPERTIES OF HEAT STORAGE MATERIALS

No.	Material	Specific Heat kj/kgK	Thermal Conductivity W/mK
46	$LiNO_3$	1.63	-
38	NaOH	1.47	1.54
26	$Ca(NO_3)_2$	0.88	-
19	Al	0.92	204.2
18	LiH	8.04	7.0
16	$MgCl_2$	0.75	-
15	Li_2CO_3	2.64	-
13	65 NaF + 23 CaF_2 + 12 MgF_2	1.17	-
12	67 LiF + 33 MgF_2	1.42	-
43	37 LiCl + 63 LiOH	0.75	-
42	7.8 NaCl + 6.4 Na_2CO_3 + 85.8 NaOH	2.51	-
34	80 LiOH + 20 LiF	2.14	2.6

Table 2.5

MATERIALS CONSIDERED FOR WATER COOLED REACTORS

No.	Material	Melt Temp. °K	Cost Factor kJ/$	Volume Factor kJ/l
1	NaOH	593	992	965
2	93.6 $NaNO_3$ + 6.4 NaCl	568	1245	435
3	95.3 NaOH + 4.7 Na_2SO_4	566	928	703
4	7.8 NaCl + 6.4 Na_2CO_3 + 85.8 NaOH	555	1234	674
5	37 LiCl + 63 LiOH	535	100	728
6	NaCl + $ZnCl_2$	533	492	469
7	23 LiOH + 77 NaOH	528	177	456
8	$LiNO_3$	527	111	883

whereas the less expensive chloride eutectic has a low volumetric heat of fusion. Since the volumetric heat of fusion is considered the more important parameter, the selected pair is:

1. $LiNO_3$
2. 37 LiCl + 63 LiOH

However, the entire group of materials, with the exception of the two at the temperature limits, would be satisfactory candidates if considered only for the pressurized water reactor. Those with low volumetric heats of fusion have low costs which tend to offset the disadvantage.

2.4.3 Selection of Materials for Supercritical Steam System

Table 2.6 shows the considered candidate materials. The first three are present only because they fall within the originally specified temperature range, which proved to be too high. The last four were not evaluated in the original selection process. The chlorides have very low volumetric heats of fusion. The five fluorides are competitive in performance with the lithium hydroxide, while sharing the two disadvantages of being eutectics and containing highly corrosive components.

In the original evaluation, the decision between the carbonate and the lithium compounds depends almost completely on their relative corrosion characteristics, since the heat of fusion of the carbonate is lower by a factor of two. From discussions with Mr. Gary Drage of the Naval Undersea Warfare Center, Mr. LeRoy Grantham of Atomics International and Mr. Worth Percival, Private Consultant, 707 Barham Down, Manchester, MO. 63011 (314-227-7923), it was determined that the lithium compounds do not present insurmountable containment problems at fusion temperatures. Reference 3 gives data on the eutectic, demonstrating that nickel corrosion rates are low enough to permit a twenty year life. Mr. Percival, citing his experience with LiOH, states that failures were caused by extraneous factors. Therefore the carbonate is eliminated.

Table 2.6

MATERIALS CONSIDERED FOR SUPERCRITICAL STEAM SYSTEMS

No.	Material	Melt Temp. K	Cost Factor kJ/$	Volume Factor kJ/l
1	52 NaCl + 48 $NiCl_2$	843	33	1585
2	$Ca(NO_3)_2$	834	-	325
3	73 LiCl + 27 NaCl	825	206	899
4	80 Li_2CO_3 + 20 K_2CO_3	763	13	818
5	LiOH	743	199	1358
6	80 LiOH + 20 LiF	700	203	1803
7	48 NaCl + 52$CaCl_2$	773	-	708
8	49 KF + 51 LiF	765	-	1180
9	11.5 NaF + 42 KF + 46.5 LiF	727	-	1132
10	NaCl + $MgCl_2$	713	-	730

The two advantages of the eutectic are the higher heat of fusion and the negligible volume change. The thermodynamic test results given in Reference 4 are questioned for three reasons:

1. Mr. Drage has found the conductivity measurements made by the same contractor are wrong.

2. The Dynatech Thermatest Department has not encountered a material for which the specific heat of the solid exceeds that of the liquid.

3. In general, the heat of fusion of a eutectic is less than that of either component.

Thus the decision is based on the relative importance of the design difficulties raised by the negative expansion versus the potential problems of handling a eutectic, where precise control of composition is critical. Since Mr. Percival has successfully designed and operated LiOH systems for a similar application over a long period of development, LiOH becomes the recommended substance.

2.4.4 Selection of Material for Gas Cooled Reactor

Table 2.7 shows the comparison among the candidate materials for use with the Gas Cooled Reactor. One of the group, $LiCO_3$, can be eliminated because of relative expense. One, MgCl, can be eliminated because it has a low volume factor with no redeeming features. Satisfactory designs can be based around any of the others.

Two, LiH and 67 LiF + 33 MgF_2, have very high volumetric heats of fusion. The low volume factor for aluminum is offset by its high conductivity, which is at least one order of magnitude higher than any of the others. That conductivity is so high that it is doubtful that the system design will be limited by heat transfer through the solid layer. There is extensive previous work to determine the properties of aluminum (Refs. 7, 8) and of lithium hydride (Refs. 9, 10, 11). Repetition is not considered to be desirable.

Table 2.7

MATERIALS CONSIDERED FOR HIGH TEMPERATURE GAS REACTORS

No.	Material	Melt Temp. K	Cost Factor kJ/$	Volume Factor kJ/l
1	67 LiF + 33 MgF_2	1019	237	2489
2	65 NaF + 23 CaF_2 + 12 MgF_2	1018	883	1582
3	$Na_2B_4O_7$	1013	2560	1214
4	Li_2CO_3	998	17	1328
5	$MgCl_2$	988	347	1012
6	LiH	956	123	2028
7	Al	933	388	1051

The two fluoride eutectics and sodium borate give a range of potential properties. As the expense of the storage material increases, the volumetric heat of fusion goes down. The final decision is based on other considerations. Sodium borate is known to be an inert material and is readily available, as indicated by the low cost, whereas the fluorides are noted for difficulty in handling and corrosiveness. Therefore, the borate is selected.

The principal difficulty expected with the borate arises from its tendency to form a glassy solid, subcooling as heat is removed. This subcooling may be as much as 200°F unless a nucleating agent is developed for this material. Thus it is essential that a study of nucleation proceed early in the development test phase for the thermal storage system.

2.4.5 Summary of Selection

The materials selected for properties testing are:

Application	Material	Melt Temperature, °K
Pressurized Water Reactor	$LiNO_3$	527
Boiling Water Reactor	37 LiCl + 63 LiOH	533
Supercritical Steam	LiOH	743
High Temperature Gas Reactor	$Na_2B_4O_7$	1015

Section 3

MEASUREMENT OF THERMOPHYSICAL PROPERTIES

3.1 Outline of Investigation

The necessary properties to be evaluated in the overall study were:

1. melt temperature or range,
2. thermal conductivity in solid and molten phases,
3. heat capacity in solid and molten phases including latent heat of fusion, and
4. density and coefficient of volumetric expansion in solid and molten phases.

For each material both reagent and commercial grades were to be evaluated over an approximate range of 100K above and below the melting points of each. The overall temperature range for the four materials was between 500K and 1050K depending upon the application of a particular material.

Standard accepted techniques were chosen for the measurement of each property, with modifications where necessary due to associated sample-related problems. Of the properties desired, the thermal conductivity, especially in the molten phase, was the one which presented the major problems and where potential errors would be greatest.

In general, the chosen salts were highly reactive both in air and with many materials. Thus special handling of materials and samples was necessary at all stages of production, assembly and measurement and in some cases special materials and techniques were required both in the fabrication of test samples and in the subsequent measurements. This latter point is not covered in detail in Section 3.3 dealing with the sample preparation procedures.

The individual methods or techniques chosen were:

1. Measurement of melt temperature or range by differential thermal analysis, in order to determine both the overall temperature range of testing and how a particular measurement was to be carried out.

2. Measurement of thermal conductivity in the solid phase by the comparative flat slab method and in the molten phase by a special modified comparative technique.

3. Measurement of specific heat, including latent heat of fusion, by adiabatic calorimetry for the two materials being studied in the temperature range 400 to 600K and by drop calorimetry for the other two higher temperature materials.

4. Measurements of density and coefficient of expansion in the solid state by a combination of dilatometry and pycnometry and in the molten phase by a buoyancy technique.

Measurements of melting point, molten density and of specific heat could be determined on the materials in the crystal or powder form. However for the solid and molten thermal conductivity and solid linear expansion determinations measurements had to be carried out on solid crystalline samples prepared from the original crystals or powders. Details are given in Section 3.3.

3.2 Details of Materials

As a result of the initial analysis described earlier the following salts were evaluated:

1. lithium nitrate
2. the 63% lithium hydroxide, 37% lithium chloride eutectic composition
3. lithium hydroxide
4. sodium tetraborate

The raw materials were obtained in sealed containers from various suppliers. A chemical analysis of each lot was also obtained prior to any measurements. Details of the sources and of the compositions of each are given in Tables 3.1 and 3.2 respectively.

3.3 Preparation of Specimens

In the preparations of the specimens, two conditions had to be met:

1. Fabricate a solid, 100% dense specimen with the proper geometry.
2. Prevent contamination of the sample material.

A survey of available materials to contain the molten salts was made to find a suitable one for each. Besides the noble metals, where costs are prohibitive, only nickel, high-nickel alloys, and some stainless steels had acceptable corrosion rates. Since molten salts will also corrode metal oxides more readily than the base material, the candidate material had to be resistant to oxidation.

Type 304 stainless steel was chosen finally for preparation of all materials. It satisfied the basic requirements and was readily available in the stock sizes required for preparation of the appropriate thermal conductivity and linear expansion samples. However during the course of the preparation of the sodium borate considerable difficulty was experienced with obtaining the release of the sample from the mold. Following various unsatisfactory experiences with the material, ATJ sulphur-free graphite had to be used for this one material. A special quartz glass had also been tried but unsuccessfully.

The thermal conductivity samples for measurement in the solid state were approximately 51 mm diameter and 10 to 12 mm uniformly thick with a 0.3 mm groove cut across each smooth flat surface. For the molten state the sample was approximately 75 mm diameter and 20 mm thick. The linear expansion samples were 6 mm diameter and 50 mm long and the ends were machined plane parallel.

Table 3.1

DETAILS OF SOURCES OF MATERIALS EVALUATED

Material	Grade	Supplier	Lot No.	Physical Description
Lithium Nitrate	Reagent	J. T. Baker Chemical Company	35815	White Crystalline
Lithium Nitrate	Commercial	Lithium Corporation of America	419-101	White Crystalline Bulk Density 1440 kg m^{-3}
Lithium Hydroxide	Reagent	Matheson,Coleman & Bell	B 8F25	White Crystalline
Lithium Hydroxide	Commercial	Lithium Corporation of America	406-27-13	White Anhydrous Powder Bulk Density 450 kg m^{-3}
Lithium Chloride	Reagent	J. T. Baker Chemical Company	405688	White Crystalline
Lithium Chloride	Commercial	Lithium Corporation of America	411-66	White Anhydrous Crystalline Bulk Density 995 kg m^{-3}
Sodium Tetraborate	Reagent	J. T. Baker Chemical Company	508555	White Crystalline
Sodium Tetraborate	Commercial	U.S. Borax Company	N/A	White Crystalline

Table 3.2

CHEMICAL COMPOSITION OF THE "AS RECEIVED" MATERIAL

	Lithium Nitrate		Lithium Hydroxide		Lithium Chloride		Sodium Tetraborate	
	Reagent	Commercial	Reagent	Commercial	Reagent	Commercial	Reagent	Commercial
Assay	99.8	99.0	99.8	95.0	99.3	98.5	99.0	99.5
Cl	.0003	.003	.01	.005			.0005	.001
SO_4	.005	.05	.05	.07	.005	.01	.001	.002
Ba	.001	-			.001	-		
Heavy Metals	.0003	-	.002	-	.001	-	.0003	.0005
Fe	.0003	.005	.002	.006	.0005	.005	.0003	.005
Ca	.013	-	-	.06	.002	.08	.001	.001
K	.001	-						
Na	.002	-	-	.07	.002	0.8		
H_2O	-	1.0			0.3	0.6		
Insolubles			.01	.01	.005	.01	.001	.003
Li_2CO_3	-	.03	-	3.0	-	.03		
PO_4							.0005	.001

Molds with the required dimensions were then fabricated. They were designed in three parts. A flat plate with a polished surface was used as a base. On this sat a cylinder of an appropriate inner diameter with the inner surface polished and tapered to simplify the removal of the sample slug. A clamping device sealed the tube and plate together. Once the specimen was cast, the base plate could be removed and the specimen pressed out of the containing cylinder.

To prepare a sample the following procedure was finally chosen. The specimen material was dried to constant weight at 110C in vacuum. Correct proportions of material were weighed out and placed in a nickel beaker and then placed into a sealed oven purged with an inert gas. The oven was then heated slowly to above the appropriate melt temperature of the particular salt. As the specimen material was being melted, the mold was heated to approximately the same temperature as the salt. The molten salt was poured carefully into the mold. The base of the mold was cooled such that crystallization occurred only on the bottom surface. The top surface was held above the melting point by a heater placed on top of the mold to create a temperature gradient through the salt. By slowly reducing the temperature, the rate of crystallization could be controlled. As soon as a suitable thickness had been crystallized, the entire assembly was allowed to cool to room temperature. The mold was then disassembled and the specimen pressed out, ready for subsequent surface preparation.

This procedure produced samples very close to theoretical maximum density with very few minute voids. All other techniques provided too many voids within a sample. Once a test material was taken out of its disposable sealed container it was handled inside plastic glove boxes in an inert atmosphere of dry argon during all phases of sample preparation, fabrication, and assembly. Additional details relative to each salt are given as follows.

3.3.1 Lithium Nitrate

The low melting temperature and corrosion rate made lithium nitrate the easiest material to mold. Large differences in density from the solid to

the molten state made it difficult to obtain a specimen free of voids. By carefully controlling the rate of crystallization, specimens 92 to 95% dense were finally fabricated.

3.3.2 63 LiOH / 37 LiCl Eutectic

This was similar to the lithium nitrate in that large differences in the density of the two phases produced voids in the cast slug. Controlling the rate of crystallization improved this situation. Each component was weighed in correct amounts and melted individually. They were poured together and mixed and allowed to solidify. The slug was crushed into a powder and then remelted in a new cup and then normal preparation procedure followed. The finished samples had a very slight greenish tinge, due presumably to oxidation reaction with the nickel in the case of melting the lithium chloride. The material was very brittle and during the course of subsequent final sample machinery and preparation a number of samples cracked before suitable test specimens were finally made available.

3.3.3 Lithium Hydroxide

Small differences in density between the two phases simplified the casting of dense specimens. However, corrosion of the mold made removal of the sample slug very difficult. The slug bound itself to the pitted surface of the mold and shattered when it was pressed out. The final solution to the problem was to machine and polish all contacting surfaces each time they were used and minimize the time that the salt remained molten.

3.3.4 Sodium Tetraborate

This presented the most serious problems in the fabrication of solid 100% dense crystalline specimens. It was found to subcool to form a glassy, non-crystalline mass. During cooling of the melt, the rates of nucleation and crystal growth in the material are greatly inhibited by the high viscosity of the melt. However if it is cooled rapidly to a temperature below the melting

point, the viscosity increases to such an extent that nucleation is totally prevented. The glassy state is preserved indefinitely.

A fully crystalline sample could not be obtained despite using cooling rates as low as 0.01C/min, the addition of crystalline material to the melt to try to increase the rate of nucleation, and the maintenance of the molten material temperature very close to its melting point for 96 hrs. Measurements were finally carried out on non-crystalline void free samples fabricated into test slugs.

As mentioned earlier ATJ graphite was used finally for preparation of the test sample in this case. After the molds had cooled the graphite pieces were broken away from the formed sample slug. The final machining and preparation of the samples had to be carried out with diamond tooling as for a normal glass.

3.4 Experimental Procedure

3.4.1 Differential Thermal Analysis

A Netzsch Automatic Reocrding DTA instrument was used for these measurements.

A small amount of the crystalline material was placed in a specially shaped nickel DDK measuring cup centered around a protected thermocouple. A similar amount of powdered Kaolin as a reference material was similarly placed in a comparison measuring cup. The outputs of the two thermocouples were connected differentially. A separate temperature measurement protected thermocouple was placed centrally between the two cups. The cups were placed at the center of a resistance heated temperature enclosure which could be heated or cooled at constant temperature rates. After allowing the system to come to equilibrium it was heated automatically at a constant rate of 5C/min and the output of the differential thermocouple recorded together with the temperature as measured by the measurement thermocouple until the measured temperature attained a value some ten to twenty degrees above the

the expected melting point or range. The whole system was cooled and a second sample measured using a temperature use of 10C/min.

The melting point was determined from the intersection of lines drawn through the portions of the temperature time curve immediately below and above the peak.

The system had been pre-calibrated with standard reference materials $KClO_4$, SiO_2 and K_2CrO_4 obtained from National Bureau of Standards. The measured melting points were within $\pm$ 0.5C of the reference melting points.

3.4.2 Thermal Conductivity

3.4.2.1 Solid Phase

The basic method is shown schematically in Figure 3.1. For the measurements Pyroceram 9606, an inert ceramic glass, was chosen as the most suitable available reference material to cover all of the materials over the total temperature range. The thermal conductivity of Pyroceram 9606 is in the range 4 to 3 W/mK over the temperature range of interest and the salts were expected to be in a similar thermal conductivity range.

In order to check the method and the apparatus a sample of Pyrex 7740 glass was evaluated using the Pyroceram reference materials. This glass is another readily available reference material having a thermal conductivity in the range 1 to 1.5 W/mK. Results over the range 100 to 500C were within $\pm$ 1.5% of the accepted values for this material. These were considered most satisfactory as qualifying the methods and techniques to be employed.

In all cases fine gauge chromel/alumel thermocouples in a high nickel alloy protective sheath having overall dimensions of 0.25 mm were fitted tightly into the fine grooves cut across the surfaces of the sample. The instrumented sample was sandwiched between two similar instrumented samples of the reference material and of similar dimensions.

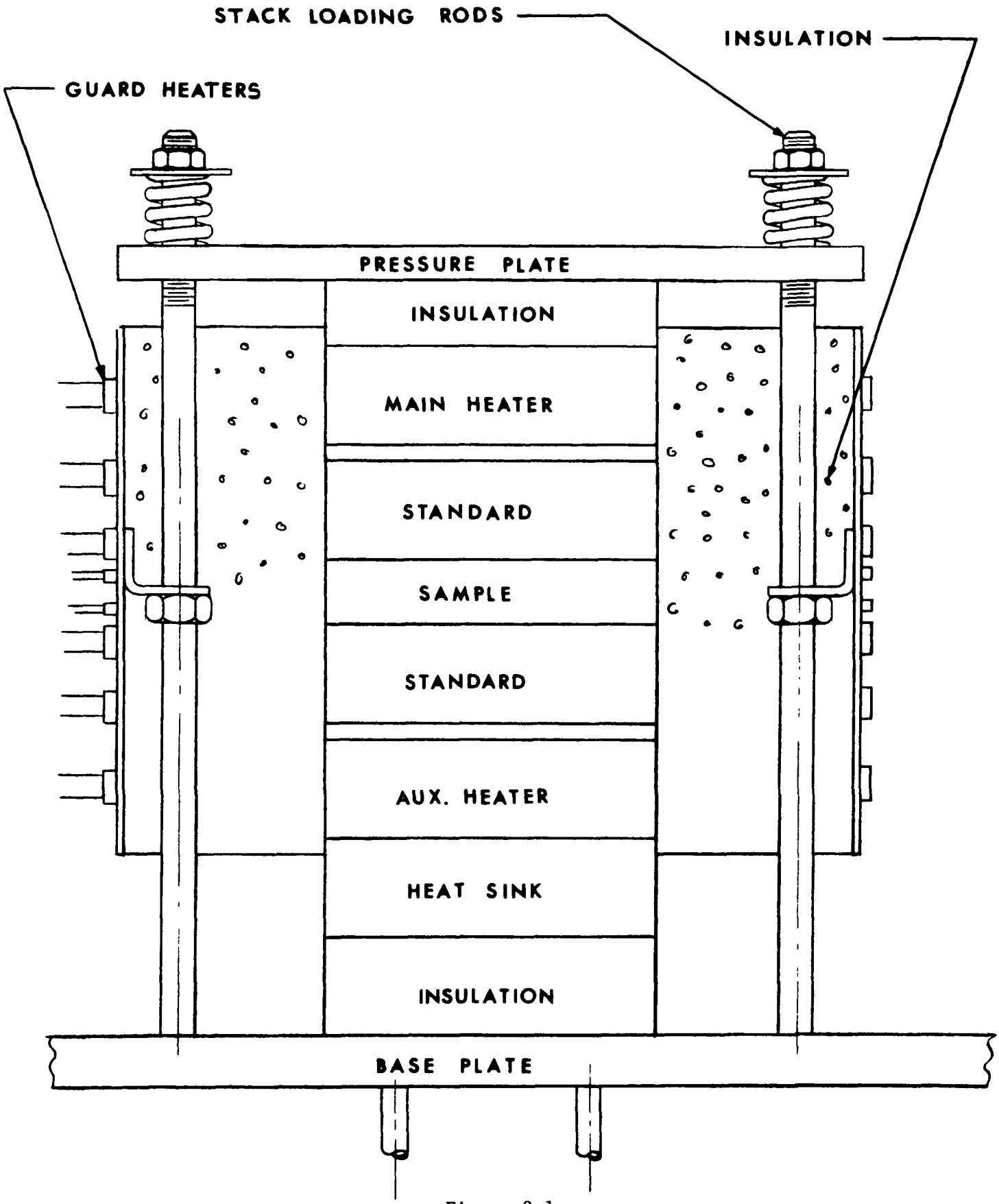

Figure 3.1

Comparative Method - Schematic Assembly

The composite sample was placed between two similar sized heater units and mounted on a fluid cooled heat sink under a uniform load applied at the top of the composite stack. A metal and ceramic heater guard tube some 75 mm diameter and 100 mm long which could be heated at various positions along its length and cooled at the bottom end was placed around the composite test stack such that the sample stack was positioned centrally with the guard tube. A further large metal fluid cooled shroud was placed around this stack and the interspaces around the sample and between the metal tubes filled with a thermal insulating powder which had been pre-dried under vacuum at elevated temperatures. A lid was fitted over the metal shroud and a large glass bell jar was placed around the whole assembly. The system was then evacuated and backfilled with pure dry argon.

A steady temperature equilibrium was established in the system by means of adjustment of the power to the heaters in the sample stack and the rate of flow of cooling water through the heat sink. The temperature gradient along the length of the guard tube was matched approximately to that on the composite test stack by automatic control of the heater along the length of the guard tube.

At equilibrium the temperatures in different sections of the stack were obtained from the various thermocouples in different sections of the stack. The thermal conductivity was derived from a knowledge of the heat flow as determined from the mean value calculated in the top and bottom reference materials, the temperature difference across the sample and the known dimensions as follows:

$$\lambda = \frac{1}{2}\left(\frac{\Delta\chi}{\Delta T}\right)_{\text{sample}}\left[\left(\frac{k\Delta T}{\Delta\chi}\right)_{\text{top reference}} + \left(\frac{k\Delta T}{\Delta\chi}\right)_{\text{bottom reference}}\right] \qquad (3.1)$$

where λ = thermal conductivity

$\Delta\chi$ = thickness

ΔT = temperature difference

k = thermal conductivities of the reference at respective mean temperatures

Measurements were made at regular temperature intervals up to as close to the melting point as could be obtained without any part of the test sample being at a temperature above the measured melting point. Following these measurements a repeat determination was made at a lower temperature to check whether the sample had changed during the heating or for possible contamination of the thermocouples.

A typical set of experimental data including temperature readings and calculation of results is given in Appendix B.

3.4.2.2 Molten Phase

The method chosen was based on the comparative technique modified for the molten state. It is shown schematically in Figures 3.2 (a) and 3.2 (b).

Essentially the test sample is contained within a thin walled cavity in a larger piece of a reference material. The bottom solid section of the material acts as the lower portion of the comparative stack while an upper section of the same reference material fits tightly into the sample cavity to seal the test sample within the cavity. The upper reference material contained a vent hole to allow for expansion of the test sample on melting and subsequent increase in temperature. Sheathed protected fine gauge thermocouples were placed in the wall of the cavity, in the surfaces of the references touching the molten material, in holes along the length of the reference materials and in the sample itself. In all other respects the experimental techniques were the same as for the solid phase.

In deriving the thermal conductivity of the molten sample the same principle was used as that for the solid material. However allowances had to be made for the heat flow through the walls of the sample container. This was found to be in the order of 20 to 25% of the total heat flow measured in terms of that in the upper and lower reference materials.

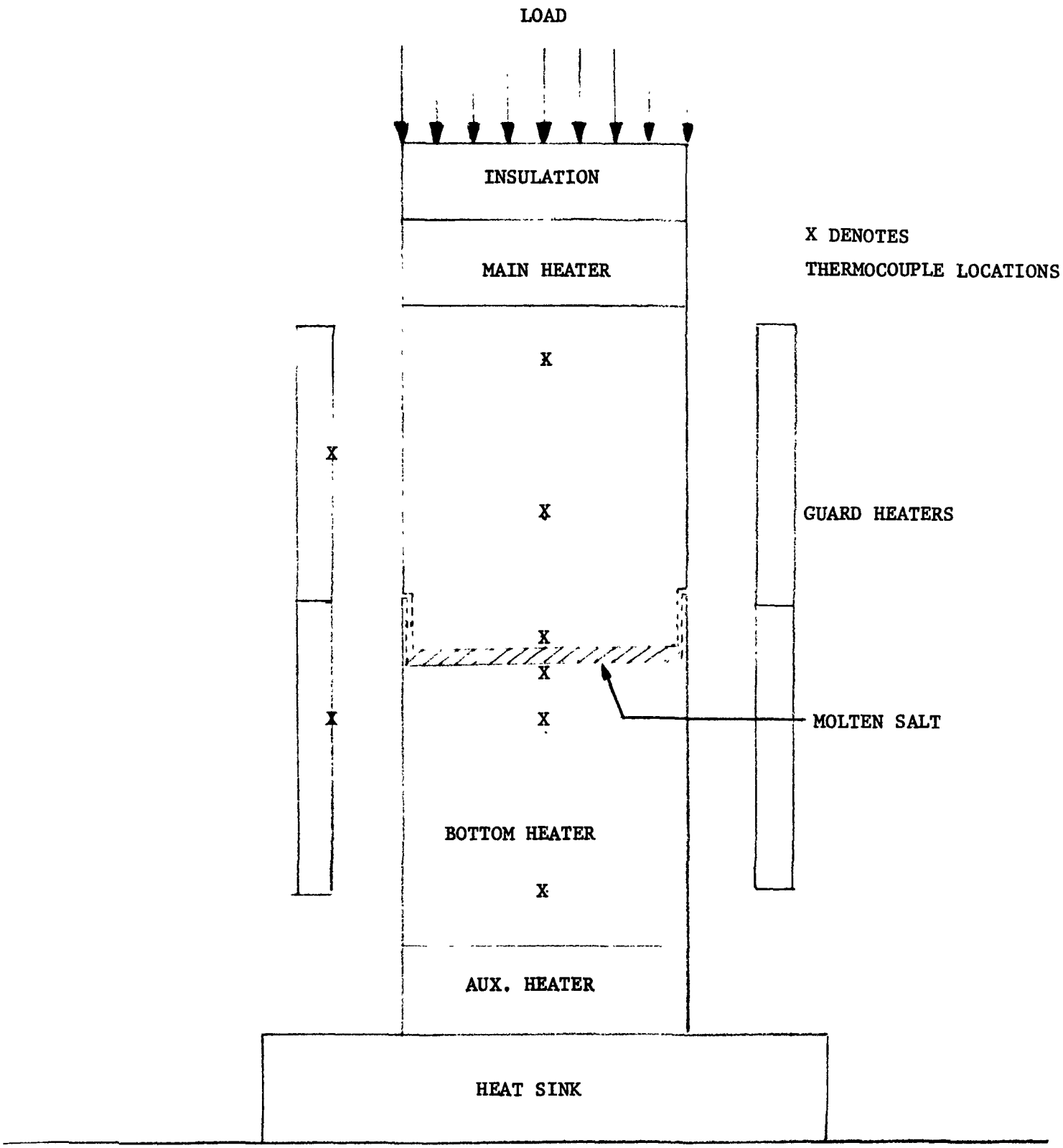

Figure 3.2 (a)

Molten Thermal Conductivity Test Stack Schematic Assembly

Numbers Indicate Positions of Thermocouples

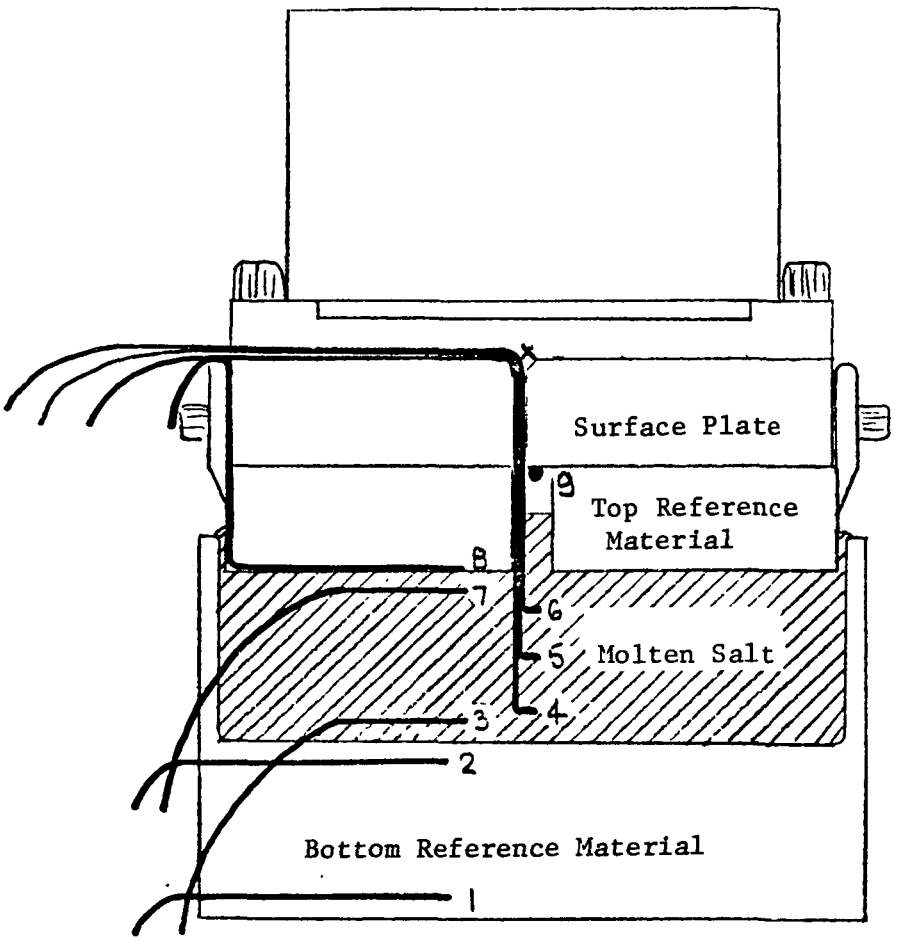

Figure 3.2 (b)

Cross-Section of Pyroceram 9606 Test Stack

For lithium nitrate and one sample of the eutectic compound a test stack fabricated from Pyroceram 9606 was used. However the container cracked and no large enough piece of Pyroceram was available at the time from which a second test stack could be fabricated. In addition it had been found that lithium hydroxide,and the eutectic compound to a lesser extent, attacked pyroceram when they were molten and were assumed to be contaminated.

A test cell of Inconel 600 was then fabricated for the measurements on the materials other than the lithium nitrate. The Inconel 600 was of much higher thermal conductivity (10 to 20 W/mK) than the Pyroceram 9606 but this factor was compensated by using a larger total cross-section and a thinner wall of the cavity. In this way the heat flow in the cavity wall was still kept to the order of 20% of the total heat flow.

For the Pyroceram test stack a sample of calculated dimensions was cast and machined for insertion into the cavity. However for the Inconel test stack a sample could be cast directly in the cavity using the technique described earlier in Section 3.3.

3.4.3 Heat Capacity and Latent Heat

3.4.3.1 Adiabatic Calorimeter

The apparatus is shown schematically in Figure 3.3.

For the lithium nitrate and the eutectic material special sample containers were fabricated and calibrated empty separately. These were fabricated from 304 stainless steel in the form of cylinders approximately 50 mm long, 23 mm diameter with a 0.7 mm wall thickness with a screw cap. A resistance heater of sheathed wire was brazed all around the tube and on the top and bottom in a uniform configuration. The internal and external surfaces of the complete unit were gold plated and polished. Once a container had been calibrated empty the specific heat of ice and water were measured as was the latent heat of fusion. Results well within $\pm$ 1% of the accepted values for this material were obtained and the apparatus was then considered suitable for measurement on the salts.

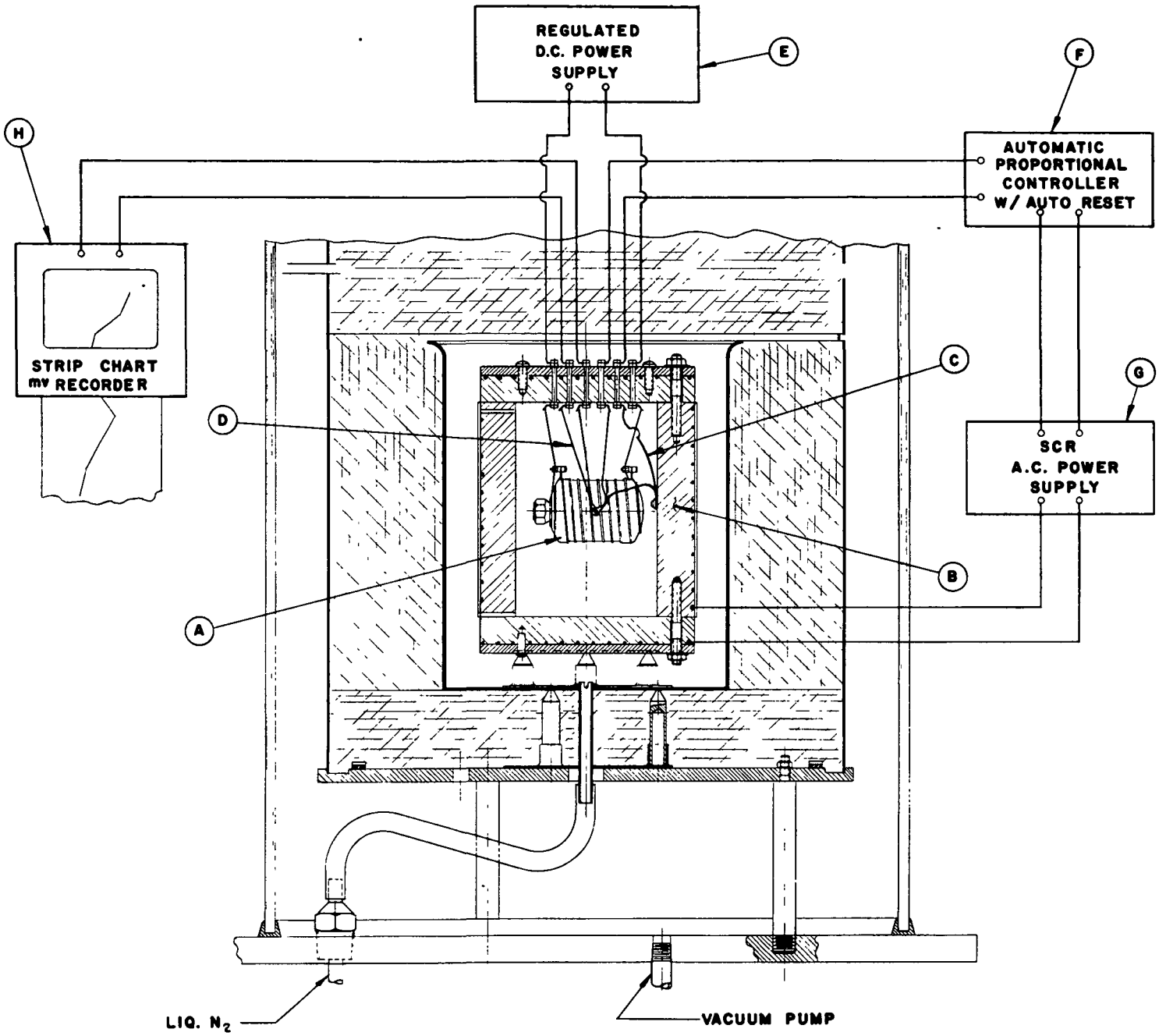

LEGEND

A SAMPLE CONTAINER - HEATER ASS'Y.

B ADIABATIC JACKET

C DIFFERENTIAL THERMOCOUPLE PROVIDING JACKET CONTROL SIGNAL

D THERMOCOUPLE FOR RECORDING SAMPLE TEMP.

Figure 3.3

Schematic Diagram of Dynatech QTA

Quantitative Adiabatic Calorimeter

A sample was melted into a container in the manner described earlier in order to maximize the amount of material being measured. The electrically heated gold-plated container was suspended inside a heavy nickel-plated and polished copper guard enclosure. The whole assembly was evacuated and then cooled at a uniform temperature below the lowest mean temperature at which data was required. When steady conditions were obtained, a controlled rate continuous power input was supplied to the heater on the sample container. By utilizing the output of a multi-junction differential thermopile, the power to the guard heater was automatically controlled so that the temperature of the guard was equal to the temperature of the sample allowing negligible heat transfer from the sample to its surroundings.

From observations of the power input to the heater and a continuous record of sample temperature variation with time, a record of the sample and container enthalpy change with temperature was obtained.

The specific heat was calculated from:

$$C_p = \frac{(mC_p)_{tot} - (mC_p)_c}{m_s} \tag{3.2}$$

where C_p = specific heat of the sample

$(mC_p)_{tot}$ = instantaneous total enthalpy change with temperature from graphical record

$(mC_p)_c$ = instantaneous container enthalpy change with temperature from the calibration graphical record

m_s = mass of sample

The latent heat of fusion was obtained from the direct measurements of the steady applied power to the sample and the time period at which the temperature remained constant.

A typical set of data and its analysis is given in Appendix B.

3.4.3.2 Drop Calorimetry

The method used was based upon typical drop calorimetry procedure utilizing a calibrated copper sample receiver contained in a constant temperature water enclosure.

Special sample containers were fabricated from 304 stainless steel in the form of thin wall cylinders some 75 mm long, 25 mm diameter and 0.7 mm wall thickness, with a threaded top cap. A container was calibrated at regular temperature intervals over the complete temperature range of the entire study and the other containers at individual points within the range. Slight differences in the overall enthalpy change for the different containers were adjusted from the knowledge of their masses.

The specific heats of a sample of each of OFHC copper and of high purity alumina were measured with use of the containers as a final calibration of the system.

For each test a sample was melted into a container as described earlier. The filled container was then attached to a 0.3 mm support wire of a nickel alloy and suspended vertically at the center of a three-zone controlled temperature furnace with the free end of the wire passing over a free moving pulley at the top of the furnace. Two thermocouples were suspended from the top of the furnace such that the junctions touched the sample near the top and bottom. The wire was so arranged that the sample was suspended vertically along the center line of the furnace and of such a length that when it came to rest at the end of its travel the sample rested upon the base of the receiver below it. Great care was taken to assure that the sample would fall quickly and freely without hitting the side of the furnace tube or the intermediate cylindrical protection tube and that it decelerated over the last 20 mm of its fall.

The sample was allowed to attain the equilibirum temperature in a dry argon atmosphere for the order of 1 - 2 hours and regular readings of the

temperature measurement thermocouples taken. During the thirty minutes prior to a "drop" the temperature of the receiver was noted every 30 s. At equilibrium when the two thermocouples and the very small drift in temperature of the receiver had been noted, the sample was dropped quickly. As the sample dropped the radiation shields covering the intermediate zone moved sideways to allow the sample to fall and come to rest in the receiver. When the sample came to rest, these shields quickly returned to the original position in order to reduce any radiation transfer of heat from the furnace to the receiver or convective and radiant heat transfer from the receiver to the outside.

The temperature of the copper receiver was taken regularly at 30 s intervals for the first thirty minutes following the drop followed by 60 s intervals for the next thirty to sixty minutes in order to determine the rise in temperature and the subsequent drift in temperature of the receiver. Following a drop, the receiver system was allowed to come to equilibrium for the order of two hours. Two similar drops for each material at each temperature were performed. A typical data point is shown in Appendix B.

Since in an adiabatic system $\Delta H_r = -\Delta H$, (3.3)

where ΔH_r = enthalpy change of the copper receiver due to sample drop at 25C

$-\Delta H$ = total enthalpy change of the sample between the drop temperature and the final receiver temperature

M_a = mass of sample

C_{pa} = integrated average specific heat of sample over temperature range T_o to T_f

T_o = temperature of sample in furnace

T_f = temperature of sample and receiver at equilibrium temperature

the calibration constant at each temperature for the copper receiver was calculated as:

$$(mC_p)_r = \frac{\Delta H_r}{(T_f - T_i)} \tag{3.4}$$

where $(mC_p)_r$ = receiver calibration

T_i = initial receiver temperature

The sample drops were made as indicated and the total enthalpy of the samples at each drop temperature was calculated as:

$$\Delta H_s = (mC_p)_r \, (T_f - T_i) \tag{3.5}$$

The total enthalpy of the samples at each drop temperature was plotted against the drop temperatures and the specific heat calculated as against the drop temperatures and the specific heat calculated as:

$$mC_{ps} = \left[\frac{dH}{dt}\right] \tag{3.6}$$

where C_{ps} = specific heat of sample at selected temperature

$\frac{dH}{dt}$ = slope of enthalpy versus drop temperature plot

m = mass of sample

The heat of fusion was obtained in the following manner:

1. Measuring the total enthalpy corrected to one receiver temperature, at two successive increasing temperatures one just below the melting point and one just above. The latent heat was derived in terms of the difference between the two values.

2. Integrating the area under the curve of specific heat versus temperature over the temperature range immediately above and below the melting point.

3.5 Linear Expansion and Density

3.5.1 Solid Phase

Originally the intention had been to use a combination of basic pycnometry and dilatometry for measuring density. However the pycnometer method utilizing the measurement of the change in volume of small chips of each material in an inert silicone calibration fluid could not be used due

to very slight reactions which took place when the salts were in contact with the fluid. In consequence the linear expansion of specimens of each type of salt, cut in mutually perpendicular directions from a large prepared solid sample, were measured in a dilatometer to enable the volume coefficient of each material to be determined. From the known mass at 20C of a given sample together with the known initial volume at 20C and its change with temperature the density at 20C and over the temperature range could be determined accurately.

For the measurement of linear expansion the initial length of a sample was measured accurately with a micrometer. The sample together with a temperature measurement thermocouple was placed in a calibrated fused quartz push rod measuring system of a Netzsch Electronic Automatic Recording Dilatometer. The system was placed at the center of a resistance heater environmental chamber and allowed to equilibrate. Power was then supplied to the heater in a regular manner such that the sample temperature increased at a constant slow rate of rise of 1 C/min up to as close to the melting point of the material as could be obtained before softening of the sample was noted. During the whole length of the experiment the continuous length and temperature changes of the sample were recorded.

The coefficient of thermal expansion of the sample was obtained as follows:

$$\alpha = \frac{\Delta L}{Lo \Delta T} \tag{3.7}$$

where α = the coefficient of linear expansion

Lo = the initial length at 20C

ΔL = the change in length for a particular temperature interval obtained from a curve of Δl versus temperature, allowance being made for the length change of the quartz system calibrated previously

ΔT = the particular temperature interval

The volume coefficient was obtained as the sum of the three respective linear coefficients. The system was calibrated using both a platinum tube and a fused quartz sample.

3.5.2 Molten Phase

The basic buoyancy method was used to determine this property. A solid cylindrical piece of nickel some 6 mm diameter and 18 mm long weighing approximately 40g at 20C was used as the suspended bob for the measurements. The expansion of a separate rod of the same nickel was measured in the Netzsch dilatometer in order to determine the change in volume of the metal bob at any particular temperature within the desired total range.

A sample of the salt was melted into a large nickel container which could be maintained at any desired temperature level. The nickel bob was suspended from the arm of a balance into the molten salt. Shields and insulation were placed around the wire and between the furnace and balance to minimize radiation, convection and updraft effects. The mass of the bob was evaluated once the system had attained equilibrium.

Measurements were made in this manner at successive increasing temperatures some 50 to 100C above the melting point.

The density of the salt was determined as follows:

$$\rho_s = \frac{\rho_{Ni}(m_{20} - m_T)}{m_{20}} \qquad (3.8)$$

where ρ_s = density of salt
ρ_{Ni} = density of nickel bob at test temperature (T)
m_{20} = mass of nickel bob at 20C
m_T = mass of nickel bob at test temperature (T)

The system was calibrated using distilled water and a high temperature silicone oil.

3.6 Results

3.6.1 Melting Point

The melting points of the particular samples of each salt tested are given in Table 3.3.

Table 3.3

MELTING POINTS OF FOUR ENERGY STORAGE SALTS

Material	Melting Point, C Measured	Published Handbook Values
$LiNO_3$ (R)	252	254
$LiNO_3$ (C)	252	
63 LiOH - 37 LiCl (R)	262	262
63 LiOH - 37 LiCl (C)	262	
LiOH (R)	470	471
LiOH (C)	472	
$Na_2B_4O_7$(R)	737	741
$Na_2B_4O_7$(C)	742	

All of the above temperatures are very close to accepted values. This factor and the initial analyses confirm the identity of the materials.

3.6.2 Thermal Conductivity

The experimental results for the solid phase of the lithium salts are shown in Figure 3.4. Values of thermal conductivity obtained from smooth curves drawn through the experimental points are given in Table 3.4. These values are believed to be accurate to better than $\pm$ 5%.

The results for each indicate that the reagent and commercial grades are very similar in property when allowance is made for density and/or crystal form. It should be mentioned here that the reagent form of the $LiNO_3$ was much less crystalline in appearance than the commercial grade whereas for the LiOH the reverse was the case.

For the LiOH in particular the differences between the two samples are the largest. The difference in density is small and in the opposite direction to that which would be expected in order to explain the variation between the

Figure 3.4 Thermal Conductivity of Three Lithium Salts in Solid Phase

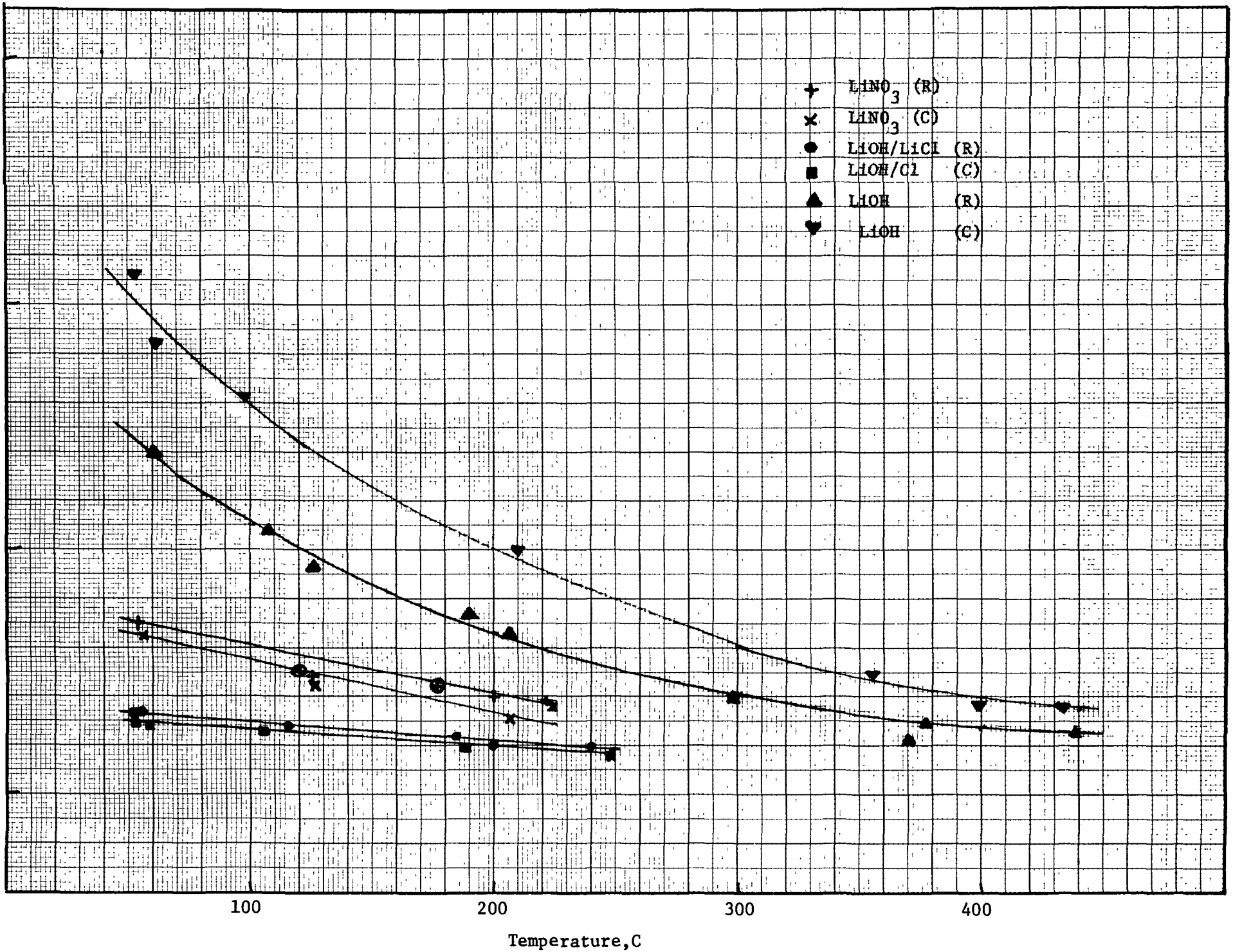

Table 3.4

THERMAL CONDUCTIVITY OF THREE ENERGY STORAGE SALTS IN THE SOLID PHASE

Specimen	Thermal Conductivity, W/mK at								
	50	100	200	225	250	300	350	400	440C
$LiNO_3$ (R) (ρ = 2139 kg/m^3)	1.73	1.53	1.40	1.38					
$LiNO_3$ (C) (ρ = 2215 kg/m^3)	1.67	1.46	1.31	1.29					
63 LiOH / 37 LiCl (R) (ρ = 1648 kg/m^3)	1.33	1.29	1.21	-	1.19				
63 LiOH / 37 LiCl (C) (ρ = 1635 kg/m^3)	1.30	1.27	1.19	-	1.17				
LiOH (R) (ρ = 1421 kg/m^3)	2.50	2.10	1.65	-	1.52	1.40	1.32	1.27	1.26
LiOH (C) (ρ = 1404 kg/m^3)	3.06	2.58	2.00	-	1.89	1.60	1.49	1.37	1.35

two samples. However for solids in general the thermal conductivity is affected markedly by crystal size and, as mentioned earlier, the commercial grade sample appeared to consist of much larger crystals than the reagent sample. One other point, the commercial grade sample was prepared from the powder form whereas the reagent grade was from the crystalline form. This again could influence the thermal conductivity of a resultant test sample.

The results for the borate material are quite different in nature to those for the lithium salt and are shown separately in Figure 3.5. Early attempts to prepare crystalline samples, coupled with results obtained in the specific heat measurement (to be discussed later) had indicated that it was not possible to fabricate crystalline solid samples and that anomalous enthalpy behavior occurred in the 500 to 600C regime. In consequence, measurements on the prepared samples in the solid state were carried out from approximately 100C up to as close to the melting point as possible.

It will be seen that above 500C there was an apparent large decrease in thermal conductivity followed by a further increase up to 700C. On dismantling it was found that a small amount of the sample in the form of beads had stuck to the sides of the lower test stack. This indicated that at some time during the measurements part of the sample had melted even though all of the sample was kept below 740C. As a consequence the thickness of the sample had changed but this was estimated to be 10 to 15%. An absolute measurement could not be made since the heat meter - sample - heat meter combination was a solidified entity and had to be broken apart and the surfaces of the heat meters remachined for the other measurements.

The 15% maximum difference in thickness is not sufficient to increase the λ value above 500C to fit to the line extrapolated through the experimental points below 500C. It would thus appear that the thermal conductivity of these samples does decrease significantly above 500C and that at some temperature between 500 and 700C limited melting of this particular form of sodium borate also takes place.

Figure 3.5 Thermal Conductivity of Sodium Borate in Solid Phase

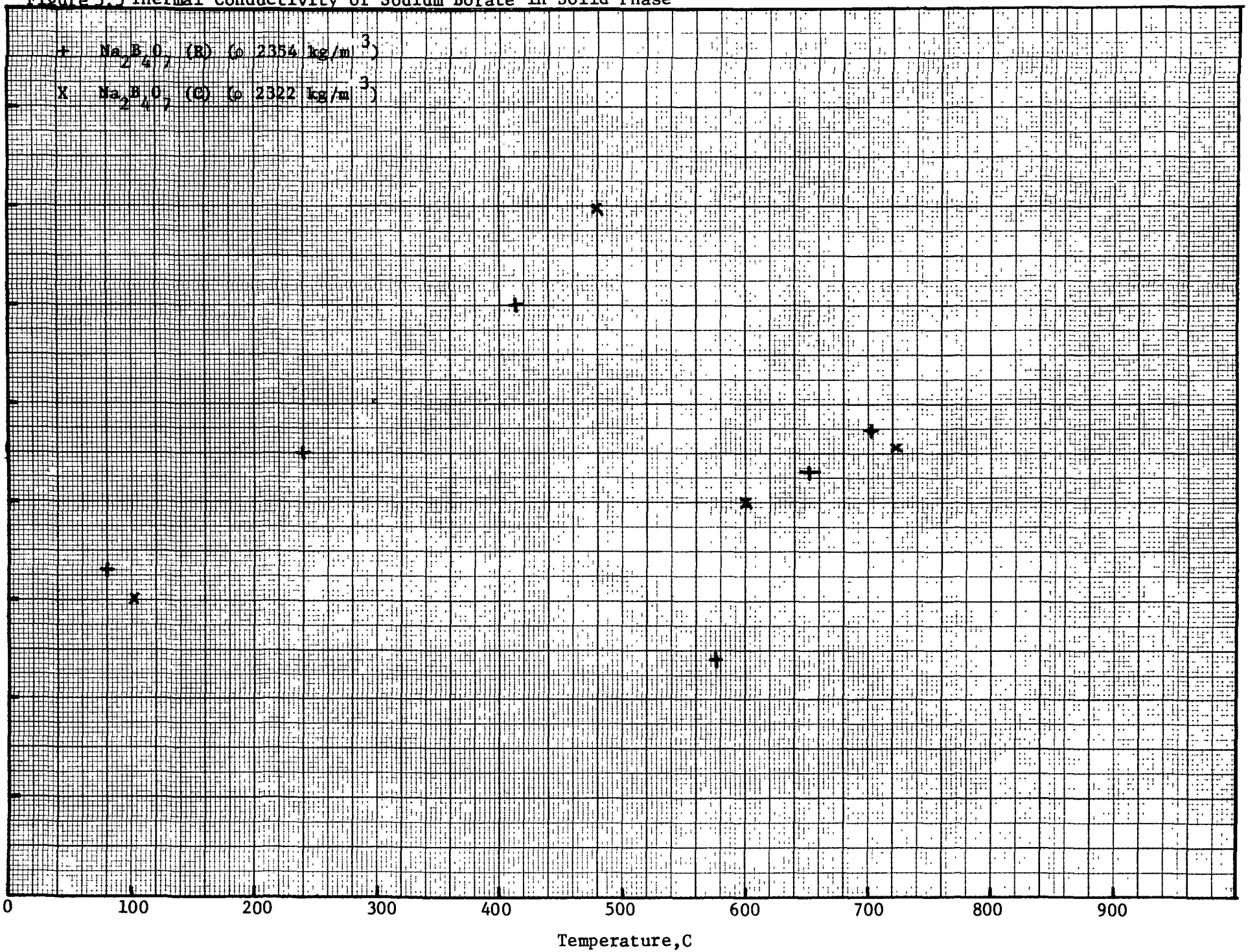

Results for the thermal conductivity of the molten phase for each material are summarized in Table 3.5. Some three data points for each material were obtained in one of the two cells described earlier.

As for the solid phase there appears to be little or no difference between the reagent and commercial grades of each material. The results for the three lithium salts indicate an approximate halving of the thermal conductivity on melting. Such a decrease is in general agreement with results for other materials, including salts, when measured in the solid and molten phases.

The discussion of the results for the sodium borate are necessarily obscured by the fact that changes in the thermal conductivity occur at temperatures below the accepted melting point. These changes occur in fabricated samples which may be of a material which has supercooled to a large extent. However if one considers the results in the 500 to 600C range there is a decrease in the thermal conductivity of the measured sample of the order of 50% as for the other materials but it is believed that not all of the sample was molten at the temperature unless the very high viscosity of the material hold the sample in place in the test stack. Some material had escaped from the test stack during the measurements but it is not known at what temperature level this occurred.

The thermal conductivity of the molten sodium borate measured in the molten cell at temperatures above 740C is similar to that measured in the solid samples at about 700C. They are believed to be representative of the molten phase. These values are only the order of 20% or so below that of the solid at 500C. However if one extrapolates the earlier result in the solid phase to 740C the reduction in value is some 30% or more. The whole question of the thermal conductivity of sodium borate remains obscure due to unknown factors which influence the form of the fabricated samples of interest particularly below 700C and above 500C.

Table 3.5

THERMAL CONDUCTIVITY OF FOUR ENERGY STORAGE SALTS IN THE MOLTEN PHASE

Material	Thermal Conductivity, W/mK			$\left(\frac{\lambda_m}{\lambda_s}\right)_{m.p.}$
	260C	300C	350C	
$LiNO_3$ (R)	0.62	0.635	0.75	0.45
$LiNO_3$ (C)	0.61	0.62	0.65	0.49

Material	Thermal Conductivity, W/mK			$\left(\frac{\lambda_m}{\lambda_s}\right)_{m.p.}$
	280C	330C	380C	
63LiOH/37LiCl (R)	0.70	0.735	0.78	0.57
63LiOH/37LiCl (C)	0.685	0.73	0.77	0.57

Material	Thermal Conductivity, W/mK			$\left(\frac{\lambda_m}{\lambda_s}\right)_{m.p}$
	490C	550C	600C	
LiOH (R)	0.85	0.87	0.88	.67
LiOH (R)	0.85	0.88	0.89	.62

Material	Thermal Conductivity, W/mK		
	760C	800C	840C
$Na_2B_4O_7$ (R)	1.07	1.09	1.1
$Na_2B_4O_7$ (C)	1.02	1.03	1.05

3.6.3 Specific Heat and Latent Heat

The results are summarized in Table 3.6. Enthalpy values for the $LiNO_3$ and LiOH/LiCl eutectic are given in Figure 3.6 and for the other materials in Figure 3.7.

The results for each material indicate that there were no differences between the reagent and commercial grades. The present values for the latent heat of the lithium salts are in very good agreement with previous measured or calculated values. The present specific heat results extend the temperature range for these materials over the complete range of use. Where previous values are available at lower temperatures the absolute values are in good agreement with the present ones. It is significant to note that the latent heat of fusion of LiOH is twice that of the other two lithium salts.

Results for the $Na_2B_4O_7$ samples do not show any indication of a significant latent heat at the nominal melting point. In fact, the results by drop calorimetry indicate a "heat of transformation" of the order of 1.5×10^5 J/kg in the vicinity of 550C. It should be realized however that these measurements were carried out on pre-melted material and thus the samples were likely to be amorphous due to possible supercooling. The nature of the drop calorimeter test, involving the rapid cooling of a sample from a fixed high temperature to a much lower one, would also give rise to further change of form or structure of a sample of this type of material.

However examination of the DTA melting point curves carried out initially on the crystalline material had indicated that some reaction took place in the 540 - 560C region besides the nominal melting at 740C. It was decided to do a more careful DTA study on new samples of crystalline material over the lower temperature range and with the melt.

A typical DTA curve is shown in Figure 3.8. It can be seen that a reaction does take place in the above lower temperature regime and that the material does melt at 740C. However, while these measurements are not accurately quantitative, it can also be seen that the heat of reaction involved at the

Table 3.6

SPECIFIC HEAT, Cp, AND LATENT HEAT OF FUSION, h_f
OF FOUR ENERGY STORAGE SALTS

Material	C_p, J/kg K at 160	200	240	260	280	300	340	400	440	550	600	700	750	800C	h_f 10^{-5} J/kg
$LiNO_3$(R)	1540	1640	2000	2050	2170	2270									5.33
$LiNO_3$(C)	1520	1620	1940	2020	2100	2210									5.28
LiOH/LiCl (R)	2100	2240	2370	2440	peak	2650	2800								4.82
LiOH/LiCl (C)	2070	2220	2340	2420	peak	2610	2750								4.88
LiOH (R)						2920	-	3150	3380	3940	3660				10.15
LiOH (C)						2730	-	3050	3190	4150	3790				11.10
$Na_2B_4O_7$(R)									1300	1400	1720	1755	1775	1795	*
$Na_2B_4O_7$ (C)									1300	1390	1700	1740	1760	1780	*

*Value could not be obtained at melting point for samples tested

Figure 3.6 Enthalpy of Lithium Nitrate and the Lithium Hydroxide / Lithium Chloride Eutecti

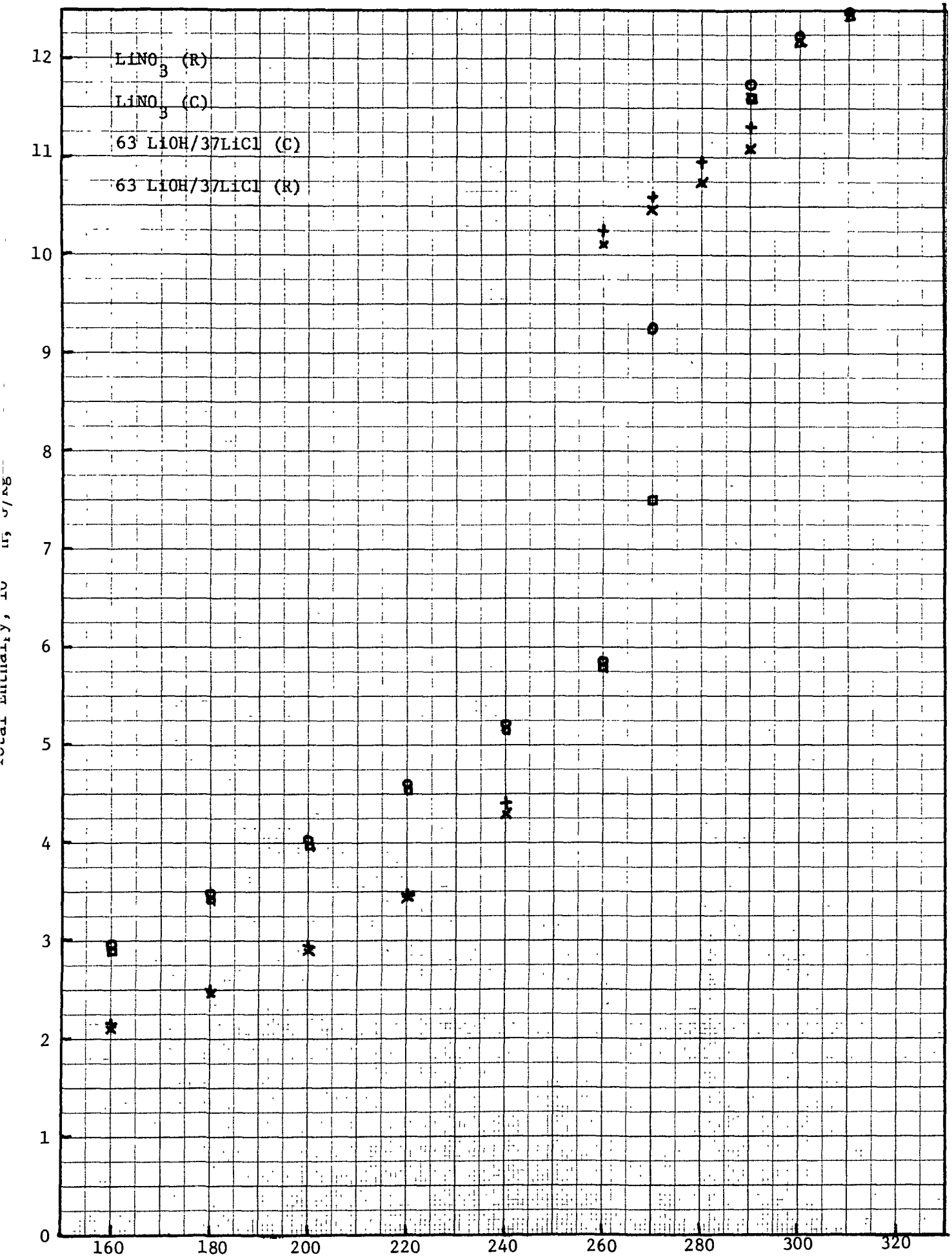

Figure 3.7 Enthalpy of Lithium Hydroxide and Sodium Borate

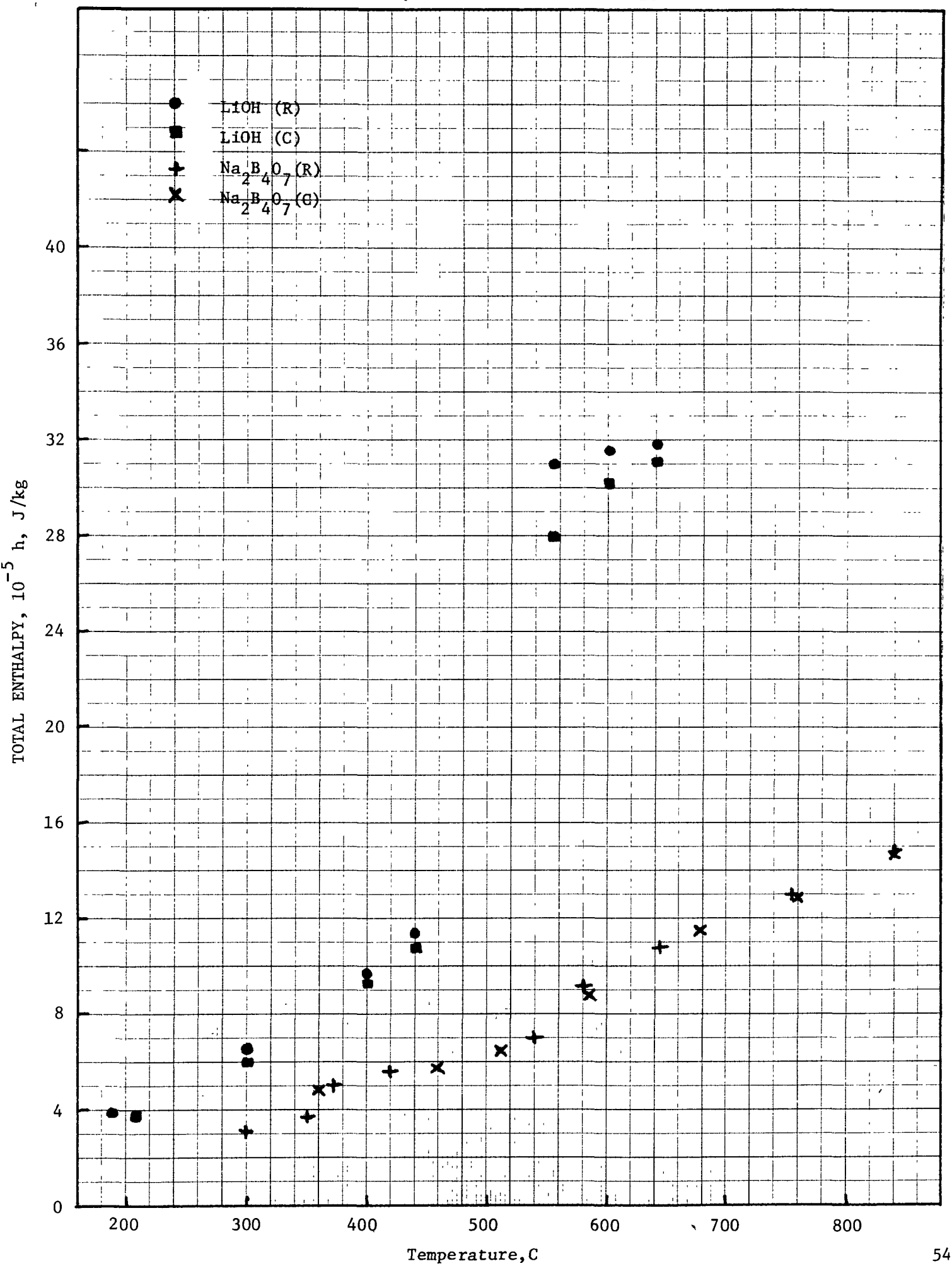

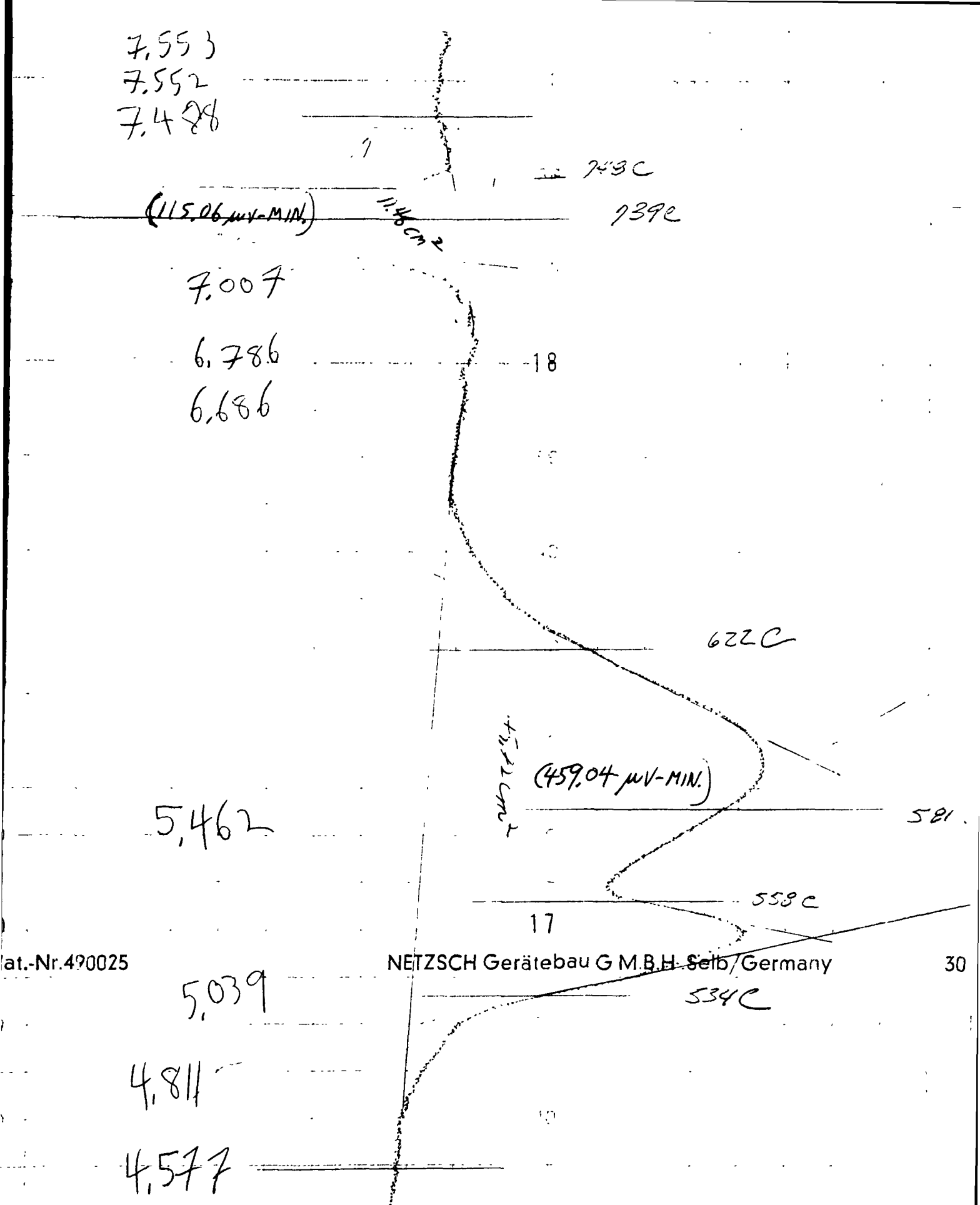

Figure 3.8 DTA Curve for Sodium Diborate

lower temperature in some four times that at the melting point. If the approximate value of 1.5×10^5 J/kg at 550C is assumed correct then the latent heat of fusion is thus only of the order of 0.4×10^5 J/kg.

After the original heating of the sample shown in Figure 3.8 had been completed it was allowed to cool very slowly to below 500C and then reheated at the standard programmed rate. The resultant curve showed no indication of any significant changes from a straight line base curve in the 550C or the 740C regimes either on cooling or reheating.

Clearly the specific heat, latent heat, and the thermal conductivity of $Na_2B_4O_7$ in the solid phase above 400C requires further study on well characterized samples if such could be made available. The present results however indicate that its use for energy storage purposes is very limited due to sample form limitations produced by different heating and cooling procedures.

3.6.4 Thermal Expansion and Density

Summarized results of the thermal expansion of the solid materials are given in Tables 3.7 and 3.8 for the parallel and perpendicular to crystal growth directions respectively. As for the other properties there is little or no difference in expansion coefficient between the reagent and commercial grades. Similarly for the $LiNO_3$ and the eutectic compound there is no significant difference in expansion behavior between the parallel and perpendicular directions. However for the LiOH and $Na_2B_4O_7$ there does appear to be a small but significant difference between the direction of each. In both cases the parallel direction is higher than the respective perpendicular direction.

Since the differences were small, an average coefficient change in length was derived for each material and the volume coefficient was assumed to be three times this value.

Table 3.7

THERMAL EXPANSION OF FOUR ENERGY STORAGE SALT MATERIALS

Specimen	Thermal Expansion, (ΔL/Lo) X10^4 Parallel to Crystal Growth										
	20C	50C	100C	150C	200C	225C	300C	400C	450C	500C	600C
$LiNO_3$ (R)	-	11.0	30.0	49.0	68.0	76.0					
$LiNO_3$ (C)	-	11.0	31.0	50.0	70.0	80.0					
63 LiOH/37LiCl (R)	-	10.0	28.0	46.0	64.0	73.0					
63LiOH/37LiCl (C)	-	8.0	22.0	37.0	53.0	62.0					
LiOH (R)	-		21.0		48.0		74.0	101.0	114.0		
LiOH (C)	-		20.0		44.0		69.0	94.0	106.0		
$Na_2B_4O_7$ (R)	-		6.0		16.5		29.4	43.5		57.4	71.1 *
$Na_2B_4O_7$	-		6.0		19.0		34.0	49.0		64.0	80.0 *

* Measurements not possible above approximately 600C due to softening of sample

Table 3.8

THERMAL EXPANSION OF FOUR ENERGY STORAGE SALT MATERIALS

Specimen	Thermal Expansion, $(\Delta L/Lo) \times 10^4$ Perpendicular to Crystal Growth										
	20C	50C	100C	150C	200C	225C	300C	400C	450C	500C	600C
$LiNO_3$ (R)	-	11.0	33.0	55.0	78.0	89.0					
$LiNO_3$ (C)	-	8.0	24.0	42.0	61.0	71.0					
63LiOH/37LiCl (R)	-	8.0	25.0	41.0	57.0	64.0					
63LiOH/37LiCl (C)	-	6.0	19.0	33.0	48.0	55.0					
LiOH (R)	-		12.0		34.0		56.0	79.0	85.0		
LiOH (C)	-		9.0		26.0		48.0	71.0	82.0		
$Na_2B_4O_7$ (R)	-		3.5		13.6		26.5	40.5		54.9	74.3*
$Na_2B_4O_7$ (C)	-		4.0		15.1		28.0	42.0		57.0	77.0*

* Measurements not possible above approximately 600C due to softening of sample

The density of each material at any temperature was calculated from the measured mean at 20C combined with the calculated volume at the particular temperature T as follows:

$$\rho_T = \frac{m_{20}}{V_T} \tag{3.9}$$

and $$V_T = V_{20}(1 + 3\alpha) \tag{3.10}$$

These calculated values of density are summarized in Table 3.9.

Table 3.10 contains values of the measured densities of the salts in the molten condition at three temperatures above the melting point. Also included are values of the ratio of the density of the melt to density of the solid at the melting point. Since the sodium borate sample softened above 600C the value of the density of the solid at the melting point has been extrapolated for the results above 600C.

Both $LiNO_3$ and the LiOH/LiCl eutectic salts have a decrease in density of 23 to 28% but the change for LiOH is 2%. However there is an apparent increase in density of some 13% for the $Na_2B_4O_7$. This again is a further factor which makes the borate material unsuitable for energy storage purposes.

In conclusion, after tests had been completed on the samples small pieces of each material were submitted for chemical analyses to see if any significant contamination had taken place. Some typical analyses are given in Appendix B.

Little significant contamination was apparent. The $LiNO_3$ and the eutectic materials contained some additional Si picked up from glass components used for part of the preparation procedure or from the silica measuring system for expansion measurements. The other elements which were present in added amounts were iron and cobalt which were probably from the alloys used in the preparation procedure. However in all cases the total amounts were very much less than 0.1%.

Table 3.9

DENSITY OF FOUR ENERGY STORAGE SALTS IN THE SOLID PHASE

Specimen	Density, kg/m^3										
	20C*	50C	100C	150C	200C	225C	300C	400C	450C	500C	600C
$LiNO_3$ (R)	2180	2173	2159	2147	2133	2128					
$LiNO_3$ (C)	2234	2227	2215	2204	2191	2184					
63LiOH/37LiCl (R)	1589	1585	1577	1508	1561	1557					
63LiOH/37LiCl (C)	1524	1520	1515	1508	1501	1498					
LiOH (R)	1434		1427		1417		1407	1396	1392		
LiOH (C)	1376		1370		1362		1352	1343	1330		
$Na_2B_4O_7$ (R)	2354		2351		2343		2334	2325		2315	2304
$Na_2B_4O_7$ (C)	2322		2318		2310		2301	2291		2280	2269

* Density of actual piece of material tested, not 100% dense.

Table 3.10

DENSITY OF FOUR ENERGY STORAGE SALTS IN THE MOLTEN STATE

Material	Melting Point C	Density, kg/m^3			$\left(\frac{\text{Solid}}{\text{Molten}}\right)$ m.p.
		280C	310C	340C	
$LiNO_3$ (R)	252	1762	1745	1726	1.30
$LiNO_3$ (C)	252	1800	1766	1745	1.26

Material	Melting Point C	Density, kg/m^3			$\left(\frac{\text{Solid}}{\text{Molten}}\right)$ m.p.
		290C	320C	350C	
63LiOH/73LiCl (R)	262	1529	1518	1507	1.23
63LiOH/37LiCl (C)	262	1527	1515	1500	1.23

Material	Melting Point C	Density, kg/m^3			$\left(\frac{\text{Solid}}{\text{Molten}}\right)$ m.p.
		500C	530C	560C	
LiOH (R)	472	1372	1359	1346	1.02
LiOH (C)	472	1381	1371	1360	1.02

Material	Melting Point	Density, kg/m^3			$\left(\frac{\text{Solid}}{\text{Molten}}\right)$ m.p.
		770C	800C	840C	
$Na_2B_4O_7$ (R)	742	2620	2607	2587	0.87
$Na_2B_4O_7$ (C)	742	2687	2670	2645	0.86

Section 4

ANALYSIS OF STORAGE SYSTEM

4.1 Power Plant

4.1.1 System Selection

The impact of thermal energy storage was assessed for one of the four power plant systems. The high temperature gas reactor was not selected since the future of this approach is in doubt (Ref. 5). Any of the other three would be a satisfactory case for study. Thermal storage is likely to provide a greater economic benefit in conjunction with nuclear systems than for the fossil fuel fired system, since the heat production capital costs for the nuclear plants are a greater portion of the total cost. Also the projection shown in Figure 2.1 indicates that nuclear power will be the dominant part of at least one system in 1990. Therefore, the boiling water reactor was selected as the system for evaluation.

4.1.2 Power Plant Specifications for Braun Sar

Power plant data were obtained from the General Electric Company (Ref. 6). The cycle description is given on Figure 4.1. The system design calls for 1250 mw, being approximately 25% larger than the size specified in Table 2.1. This gives the design specification of Table 4.1.

Table 4.1

STORAGE SYSTEM DESIGN SPECIFICATION

	Absolute	% of Daily Base Load
Base Load Plant, MW_e	1250	100%
Peaking Power Rate, MW_e	250	20%
Storage Capacity, MW_e-hr (Electric)	480	2%

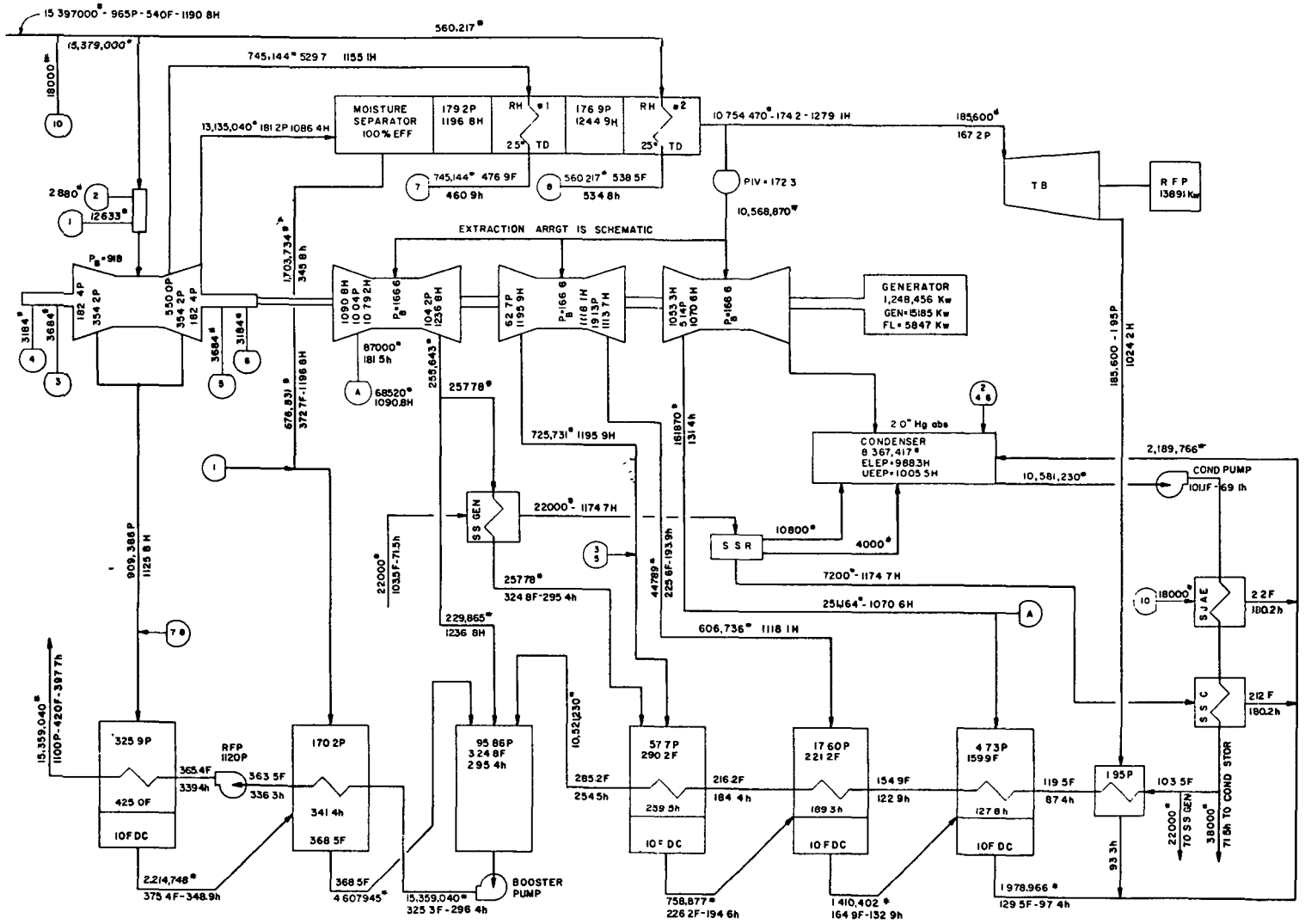

PRELIMINARY

CALCULATIONS BASED ON ASME 1967 STEAM TABLES

Figure 4.1

TURBINE CYCLE HEAT BALANCE (GE)
October 8, 1974

4.1.3 Storage System Integration

The cycle integration between the power plant and the storage system was investigated for two different modes of storage operation. In one case storage was assumed to occur over the period of five hours with a decrease in power plant output to supply the required heat input. In the other, there was a constant heat input to storage.

Two cycles were investigated for the first case and are shown in Figures 4.2 and 4.3. The low pressure power turbine was operated at the design condition. Therefore, the power output of the low pressure turbine is the same, at 840 MW_e. Thus the loss in equivalent power to supply the storage is 410 MW_e. In both cycles all bleeds and feed water heaters associated with the low pressure turbine were maintained, and the steam to the storage system was condensed and returned to storage. The reactor output rate had to be increased since the enthalpy of the return stream was decreased. If the enthalpy of the return stream were maintained to keep reactor capacity level, the thermal energy to storage would equal the power loss from the high pressure turbine.

In both cycles the steam flow to the low pressure turbine was throttled from reactor outlet. In Cycle 1 part of the remainder went to storage and part went through the system reheater to increase the temperatrue of the throttled steam to the design temperature. In Cycle 2, the entire remainder went to storage and the liquid condensate leaving the storage system was used to superheat the steam entering the low pressure turbine. Schematics for the two systems are shown on Figures 4.2 and 4.3. The performance is given in Table 4.2.

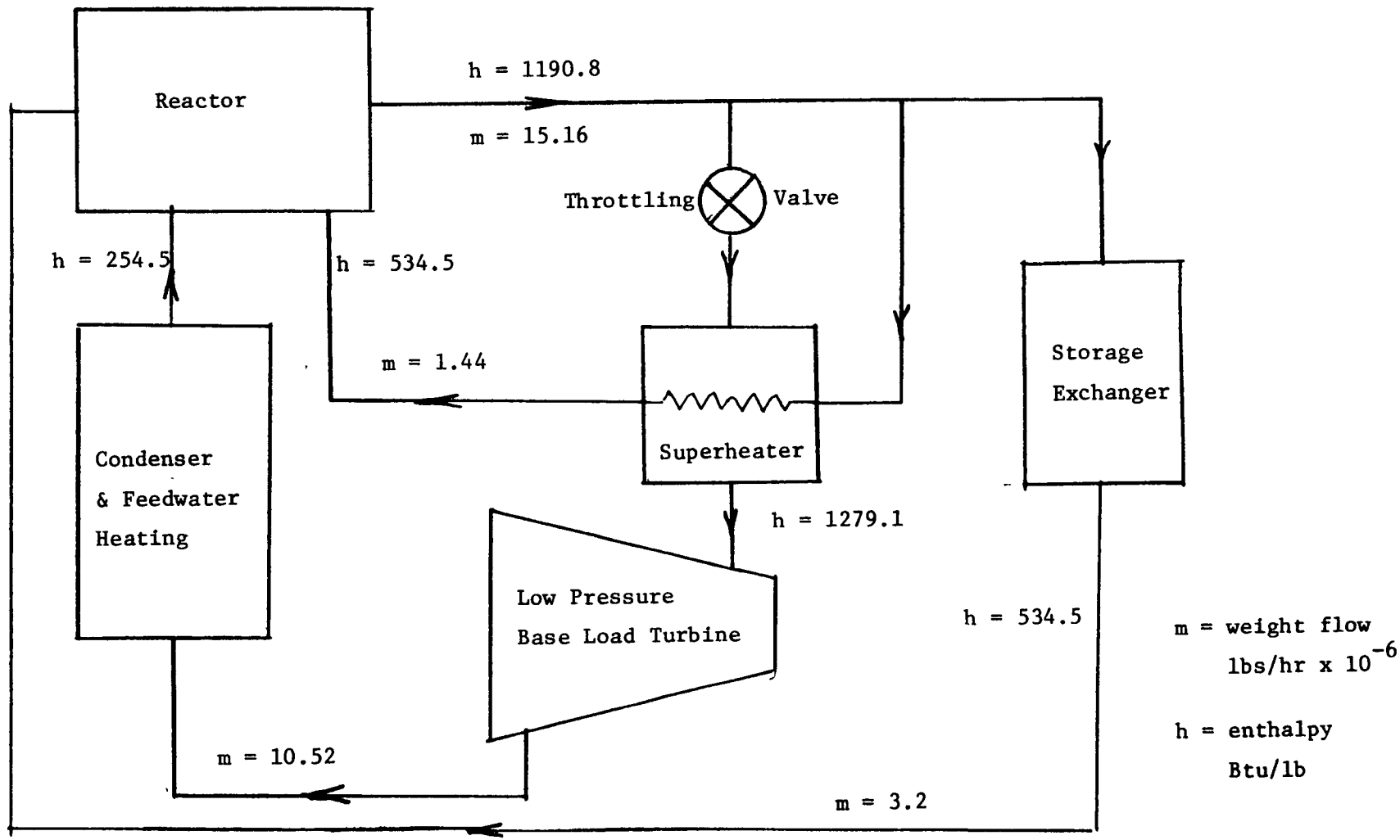

Figure 4.2

Schematic and Heat Balance - Cycle 1

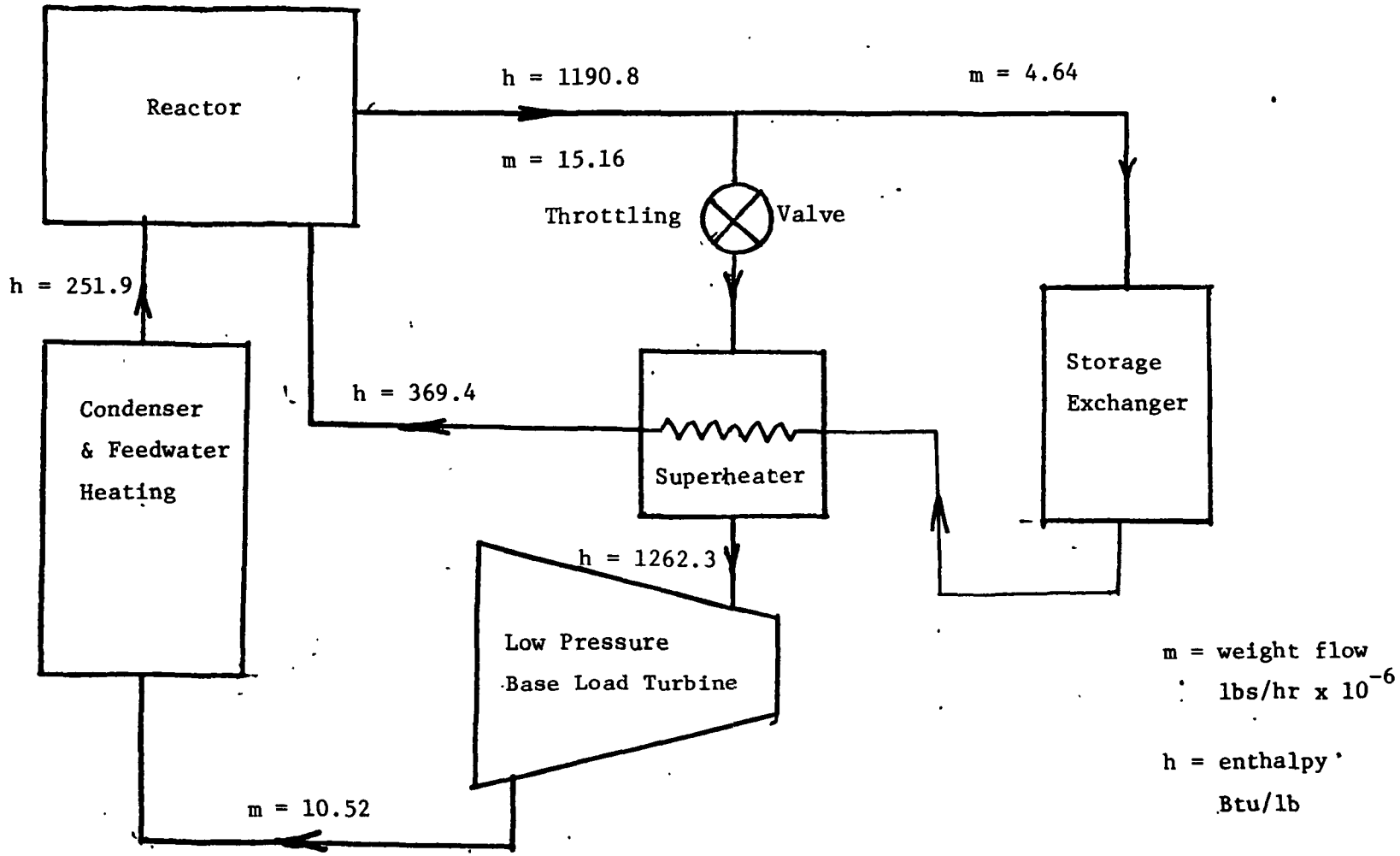

Figure 4.3

Schematic and Heat Balance - Cycle 2

Table 4.2

EFFECT OF THERMAL STORAGE ON CYCLE OPERATION

		Off Peak Storage	
	Base Load	Cycle 1	Cycle 2
Power Output, MW_e	1250	840	840
Reactor Heat Input, MW_e	3580	3775	4010
Heat to Storage, MW_e	0	615	890
Equivalent Diurnal Electric Storage, 5 hrs Cycle, 25% Efficiency, MW_e-hr	-	770*	1100*
Overall Efficiency	.359	.265	.263

* Cycle efficiency; # MW_e-hr assumes about 65% of available thermal energy can produce useful output electrical energy (Ref. 1, Table 1).

Both of these methods of integrating storage reduced the efficiency of the basic power system as well as imposing the conceptual inefficiency associated with storage.

In the other mode of providing the storage the thermal output of the nuclear reactor was increased by 3% to supply the storage capacity. The flow rate corresponding to the second condition is given by:

$$W_{pv} = \left[\frac{3.412142\ Q_t - 0.033\ h_{pv} + 16.2}{h_{pv} - h_{fw}}\right] \times 10^6 + 33{,}000\ \text{lb/hr} \qquad (4.1)$$

where W_{pv} = vessel output steam flow (lb/hr)
Q_t = core thermal power (MW_t)
h_{pv} = vessel output steam enthalpy (Btu/lb)
h_{fw} = feedwater enthalpy (Btu/lb)

(Cycle data will be given in English units as supplied by General Electric. Only the final design data will be supplied in the metric system!) The schematic on Figure 4.4 shows the cycle operating conditions.

Based on the discussion in Section 4.1.1 about the unlikelihood of reduction of power on nuclear systems, the cycles shown on Figures 4.2 and 4.3 were eliminated. It appears more feasible to overrate the system by a small amount continually in order to provide a large peak load capacity.

Thus the storage system will receive heat at the rate of approximately 100 MW continually. It will supply heat at the rate of approximately 800 MW during a peaking period of approximately two and a half hours.

4.2 Evaluation of Materials

The appropriate thermal and transport properties of the candidate materials for the four systems were determined and the results presented in Section 3. Three of the materials are viable candidates, as shown in Table 4.3.

The fourth material, sodium borate, proved to be a completely unsatisfactory material for use in thermal storage, insofar as could be told by basic properties measurement of the pure material. When the material was initially heated from room temperature in the crystalline state there was a transition to an amorphous solid at approximately 820°K, with an associated change in enthalpy, and change in thermal conductivity. The heat of fusion associated with the actual heat at 1010°K was much less than this.

Once this initial transition occurred the material stayed in the amorphous state with no phase changes of any kind and thus with no heat of fusion. Some difficulty with fusion had been expected but not this much.

Based upon the properties parameter LiOH and $LiNO_3$ are approximately equal as candidates for thermal storage materials. Both are superior to the eutectic. Therefore $LiNO_3$ is selected for system design at the specified temperature level.

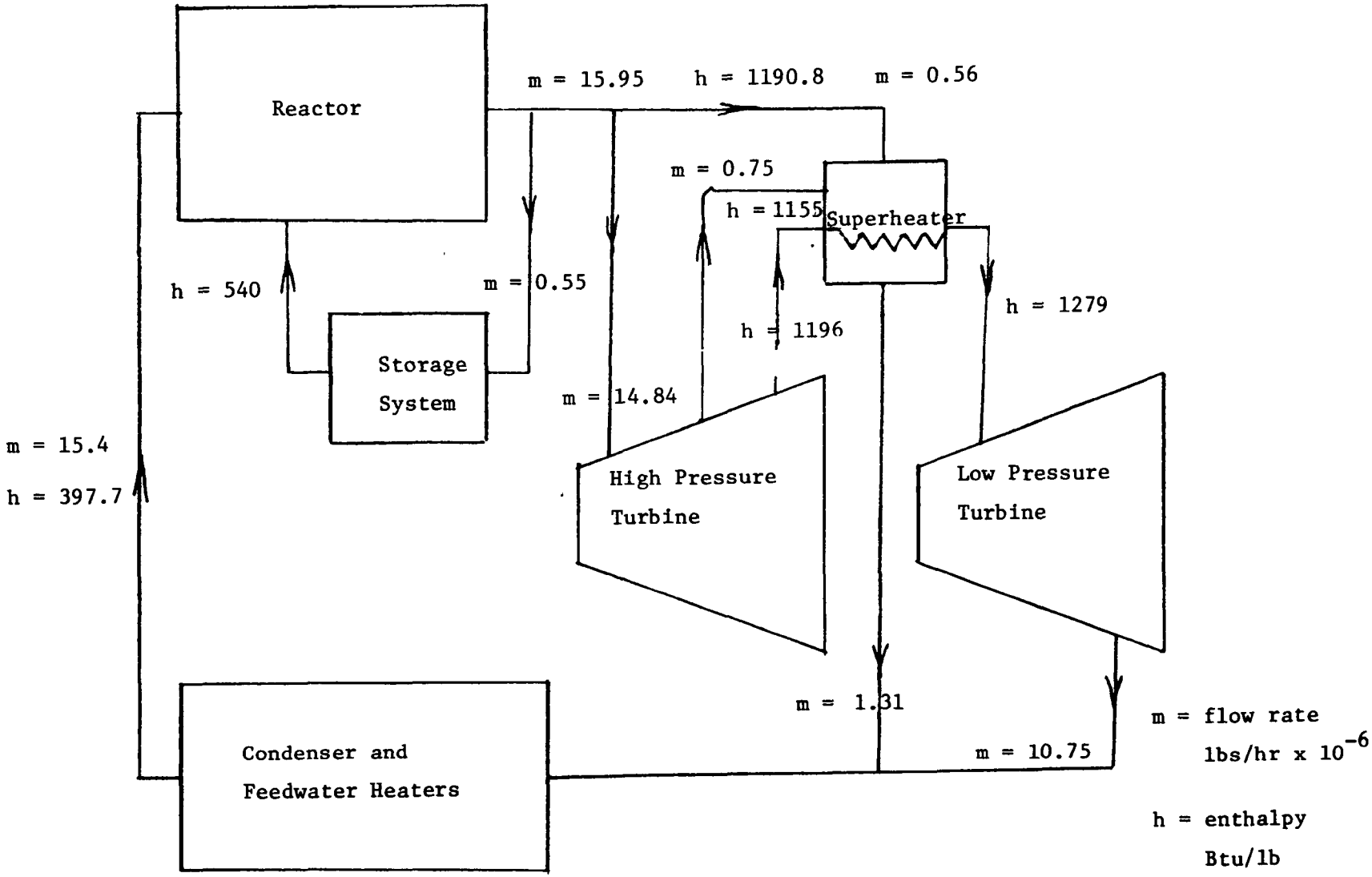

Figure 4.4

Constant Heat Supply System

Table 4.3

SUMMARY OF MATERIAL PROPERTIES

Material		$LiNO_3$	LiOH/LiCl	LiOH
Melt Temperature °K		527	535	743
Density ρ, kg/l	Test	2.310	1.900	1.415
	Postulated	(2.4)	(1.64)	(1.46)
Heat of Fusion h_F, J/kg	Test	530	485	1080
	Postulated	(379)	(437)	(930)
Thermal Conductivity λ, W/mK		1.37	1.10	1.20
Volume Product ρh_F, J/l	Test	1224	922	1486
	Postulated	(910)	(717)	(1358)
Properties Parameter $\sqrt{\lambda h_F \rho}$		41	32	42

4.3 Storage System Design

4.3.1 Specification

The storage system design will be based on Figure 4.4. The storage system will continually receive heat from the power system in the form of a steam bleed. During the peaking period of 2.7 hours the system will receive water from the peaking power system. System design operating conditions are shown on Figure 4.5.

Steam will flow through a recuperator containing static heat of fusion material. During heating the steam side is maintained at reactor pressure and the heat of fusion material is liquefied. During the power cycle the steam pressure is dropped to the low pressure turbine pressure and the heat of fusion material is solidified, while supplying heat to the low pressure system. The bypass steam flow is maintained at all times, being throttled to mix with the peaking steam flow during peaking operation. Make up condensate from the peaking cycle must be pumped into the reactor circuit to maintain liquid quantity.

With this design configuration the specification for the heat transfer system is given in Table 4.4. Table 4.4 shows the peaking period is controlling and decides the heat exchanger size. It also shows that the design is well balanced, unless there is natural convection in the liquid forming the liquid side heat transfer.

4.3.2 System Design

The heat exchanger design can be based on material inside the tubes, in a flat plate heat exchanger, or outside of the tubes.

4.3.2.1 Storage Tubes Design

With an idealized design the tubes will be sized to contain the precise amount of volume when liquefied. This specified the ideal radius ratio at the end of the solidification. Using this ratio the diameter and length of tubes could be determined.

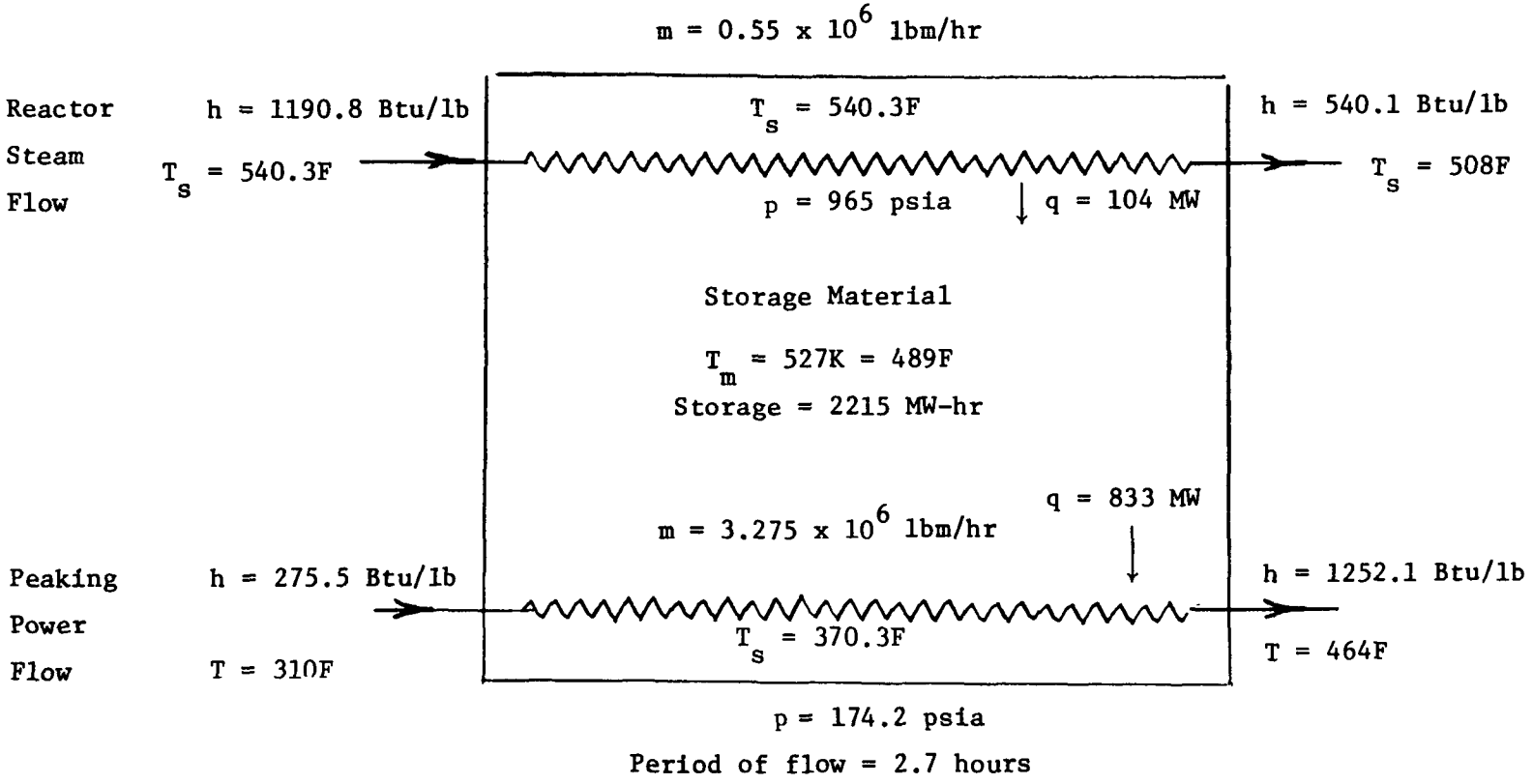

Figure 4.5

Storage System Design Specifications

Table 4.4

STORAGE DESIGN CONDITIONS

Capacity	2215 MW-hr	
Heat of fusion, J/kg	0.53×10^6	
Period	Storage	Peaking
Heat load, MW	104	853
Temperature difference, °K	28	66
Time, hr	21.3	2.7
Density, kg/m^3	1800	2310
Thermal Conductivity, W/m °K	0.62	1.37
Area, m^2	$.224 \times 10^6$	$.243 \times 10^6$
Design melt thickness, m	.0374	.0268

$$\frac{r_i}{r_o} = \sqrt{1 - \frac{\rho_\ell}{\rho_s}}$$

$$= \sqrt{1 - \frac{1.8}{2.31}}$$

$$= 0.47 \qquad (4.2)$$

From Equation A.10:

$$r_o = \sqrt{\frac{2\lambda \Delta T t}{h_F \rho \left[1 - (r_i/r_o)^2\right] \ln\left[r_o/r_1\right]}}$$

$$= \sqrt{\frac{2 \times 1.37 \times (530 - 461)\ 2.7 \times 3600}{.53 \times 10^6 \times 2400(1 - .47^2)\ln(1/.47)}}$$

$$= .05 \text{ m } (\sim 2 \text{ inch})$$

Lithium nitrate did not demonstrate any of the corrosion problems associated with lithium hydroxide and lithium chloride. Therefore, stainless steel tubing rather than inconel is specified with an eighth inch wall (0.32 cm) leaving an inside diameter of 1.75 in, with a ten percent margin of error on the design diameter to allow for shell side thermal resistance.

The total amount of tubing required is specified by the liquid volume. The total volume required is given by:

$$V = \frac{Q}{h_F \rho_\ell} = \frac{833 \times 10^6 \times 2.7 \times 3600}{.53 \times 10^6 \times 1800} \times 1.1 \qquad (4.3)$$

$$= 9550 \text{ m}^3$$

The total length of heat of fusion tubing is:

$$\frac{V}{A} = \frac{9550}{\pi(.05)^2} = 1.22 \times 10^6 \text{ m} \qquad (4.4)$$

The shell volume for center to center triangular spacing of 1.125 times the outer diameter is:

$$V_s = V \frac{S^2}{Di^2} \frac{6}{\pi\sqrt{3}} \tag{4.5}$$

$$V_s = 9550 \times \left[\frac{1.125}{.875}\right]^2 \frac{6}{\sqrt{3}\pi}$$

$$= 17407 \text{ m}^3$$

With a tube length of 50 meters, the pressure vessel diameter becomes:

$$D = \sqrt{\frac{V \cdot 4}{L\pi}} \tag{4.6}$$

$$= \sqrt{\frac{17407 \times 4}{50\ \pi}}$$

$$= 21 \text{ meters}$$

This is not feasible even with a number of vessels.

4.3.2.2 Design with Steam in Tubes

With steam inside the tubes there is no limitation on the radius ratio in Equation A.10. As smaller tubes are selected the area requirement for heat transfer becomes smaller and thus less expensive. Thus an arbitrary design radius selection of .0125 m (1 inch O.D.) was made with a .0025 m wall. For design purposes the steam side heat transfer coefficient was assumed to be 2500 W/m^2 °K ($\sim$ 500 Btu/hr ft^2 F) with a stainless steel thermal conductivity of 19 W/m°K. This reduced the effective driving temperature difference for solidification in Equation A.10 by the temperature difference required to transfer 833 MW through these two resistances at the given area. Equation A.10 was solved by trial and error for the radius ratio of the solidifying interface at the end of the peaking period. Then the area was determined from Equation A.9 and used to define the difference more precisely. The final

resulting design was:

Tube outer diameter	0.025 m
Radius ratio at maximum solid layer diameter	3
Tube area	133,600 m^2
Tubing length	1.7×10^6 m

The recommended tubing area would be triangular staggered with the minimum tube to tube spacing being determined by liquid volume corresponding to the solid mass frozen. If at least this much space is not provided there would be a possibility of liquid being trapped within a solid mass and imposing an excess stress on the tubes. Thus the minimum tube to tube spacing (D_s/D_o) is specified by:

$$\frac{D_s}{D_o} = \sqrt{\frac{\pi\sqrt{3}}{6}\frac{\rho_s}{\rho_\ell}\left[\left(\frac{r}{r_o}\right)^2 - 1\right] + 1} \qquad (4.7)$$

$$= \sqrt{\frac{\pi\sqrt{3}}{6}\frac{2310}{1800}\left[(3)^2 - 1\right] + 1}$$

$$= 3.21 \text{ (use } 3.25)$$

With this spacing the total volume required for the tube bank is:

$$V = r_s^2 \frac{6}{\sqrt{3}} L \qquad (4.8)$$

$$= (3.25 \times .0125)^2 \frac{6}{\sqrt{3}} 1.7 \times 10^6$$

$$= 9720 \text{ } m^3$$

In addition, an excess liquid level must be provided to cover the top of the tubes at all times. This is equal to the volume difference between the liquid and solid volumes of the active storage volume:

$$V = \pi r_o^2 \left[\left(\frac{r}{r_o} \right)^2 - 1 \right] L \left(\frac{\rho_s}{\rho_\ell} - 1 \right) \tag{4.9}$$

$$= \pi(.0125)^2 \, (3^2 - 1) \, 1.7 \times 10^6 \left(\frac{2310}{1800} - 1 \right)$$

$$= 1890 \text{ m}^2$$

The total mass of material required is:

$$m = (V_t - \pi r_o^2 L)\rho_\ell$$

$$= \left[1890 + 9720 - \pi(.0125)^2 \, 1.7 \times 10^6 \right] \times 1800$$

$$= 19.2 \times 10^6 \text{ kg}$$

REFERENCES

1. F. D. Kalhammer, Impact of Energy Storage on Electric Power Systems, American Nuclear Society Meeting, San Francisco, Calif., November 17 - 22, 1975.

2. Joyce, J., Telephone Conversation, July 14, 1975.

3. De Vries, Gerrit, and L. F. Gunther, "Corrosion of Metals in the Molten LiOH - LiF Water System", Electrochemical Technology, Vol. 5, No. 7 - 8, July - August, 1967.

4. Drage, Garig, D., Gerrit De Vries, and H. F. Karig, Eutectic Molten Salt Thermal Storage System, NUWC TP74, Naval Undersea Warfare Center, Pasadena (San Diego), California, September 1968, AD840279.

5. W. McCarter, Wall Street Journal, Wednesday, February 25, 1976, p. 1.

6. Hoffman, Shirley, General Description of a Boiling Water Reactor, Nuclear Energy Divisions, General Electric Co., San Jose, California, 93125.

7. Powell, R.W., Tye, R.P. and Metcalf, S.C., Advances in Thermophysical Properties at Extreme Temperatures and Pressures, 3rd Symposium on Thermophysical Properties, ASME, 277-95, 1965.

8. Pochapsky, T.E. "Heat Capacity and Resistance Measurements for Aluminum and Lead Wires", Acta Metallurgica, Vol. 1, No. 6, Nov. 1953, pp. 747-51.

9. Callery Chemical Company, "Determination and Analysis of the Potentialities of Thermal Energy Storage Materials", ASD Technical Report 61-187 (1961).

10. Gibb, T.R. P., Jr. and Messer, C.E., "A Survey Report on Lithium Hydride", AEC Rep. no. NYO-3957, 1954.

11. "A Compendium of Data on Lithium and Selected Compounds of Lithium", Lithium Corp. of America, Inc., Feb. 1958.

Appendix A

DERIVATION OF AREA CRITERION

The solidifcation rate of a pure substance on a solid interface, when the interface is maintained at a constant temperature, depends upon the rate of heat transfer through the solid layer. The liquid can be treated as a well stirred fluid, with relatively little heat transfer to the superheated liquid. The sensible heat transfered to the subcooled solid is small as compared to the heat of fusion. As a first approximation in the following analysis it is neglected. A more precise, slightly conservative, approach would be to consider the sensible heat in the solid layer as being generated at the solidification face. This quantity, which closely approximates one-half the product of the solid specific heat and the temperature difference between melt and surface, can be added to the effective heat of fusion.

The heat flux at the solidifying face is:

$$q/A = \rho h_F \frac{dx}{dt} \tag{A.1}$$

With the assumptions specified above:

$$q/A = \frac{\lambda}{x} (T_m - T_s) \tag{A.2}$$

Combining A.1 and A.2 gives:

$$\frac{dx}{dt} = \frac{\lambda}{x} \frac{(T_m - T_s)}{h_F \rho} \tag{A.3}$$

Integrations over a period of time (t) give a thickness:

$$\int_0^{\Delta} x dx = \frac{\lambda (T_m - T_s)}{h_F \rho} \int_{t_0}^{t_1} dt \tag{A.4}$$

$$\frac{\Delta^2}{2} = \frac{\lambda (T_m - T_s)}{h_F \rho} (t_1 - t_0) \tag{A.5}$$

Thus the solid thickness as a function of time for these conditions is:

$$\Delta = \sqrt{\frac{\lambda(T_m - T_s)(t_1 - t_0)}{h_F \rho}} \tag{A.6}$$

The total amount of heat transfered, as determined from the total thickness solidified is:

$$\frac{Q}{A} = h_F \rho \Delta$$

$$= \sqrt{\lambda h_F \rho (T_m - T_s)(t_1 - t_0)} \tag{A.7}$$

Thus the total amount of heat transfered through a solidifying layer is proportional to the product of properties grouping, $\sqrt{\lambda h_F \rho}$, and system design conditions. Obviously this approach to system analysis is simplistic since there will be an interaction between the rate of heat transfer at any instant in time and the interface surface temperature. However, it does separate the effect of material properties for the purpose of a first cut at material selection.

In the analysis of solidification on or in a tube, an explicit solution cannot be developed. If the limiting case is at the completion of solidification, the heat transfer rate is:

$$\frac{q}{A} = \frac{\lambda \Delta T}{r_o \ln(r_o/r)} \tag{A.8}$$

The total heat transfer is:

$$\frac{Q}{A} = \frac{h_F \rho (r_o^2 - r^2)}{2 r_o} \tag{A.9}$$

This produces an implicit function for the radius ratio:

$$\left[1 - (r/r_o)^2\right]\left[\ln(r_o/r)\right] = \frac{2\lambda \Delta T t}{r_o^2 h_F \rho} \tag{A.10}$$

The area is inversely proportional to the function of the thermal conductivity:

$$A = \frac{qr_o \ln(r_o/r_1)}{\lambda \Delta T} \qquad (A.11)$$

Thus, although the properties enter in the same manner as for the rectilinear use, it can not be demonstrated that the simple form of the properties parameter applies.

APPENDIX B

Test Data and Analysis

DYNATECH CORPORATION

DATA REDUCTION SHEET

Thermal Conductivity by Comparative Method

Temperature Point: 390 C

Project: NAS-58-1

Sample Designation: STC-3 (LiOH R)

Thickness, X_s : ( ) - ( ) = (1.589) cm

Bottom Heat Meter Material: PYROCERAM 9606

Thickness, X_{BHM}: ( ) - ( ) = (1.198) cm

Top Heat Meter Material: PYROCERAM 9606

Thickness, X_{THM}: ( ) - ( ) = (1.198) cm

Thermocouple Material: K

Avg. of (how many) readings: 3

Data of (date): 9 Dec 75

T/C No	Readings, Mv.	°C
1	13.719	336.31
2	14.214	348.14
3	14.208	348.00
4	16.058	392.00
5	16.190	395.14
6	16.722	407.74
7	15.254	372.90

Average Temperatures

BHM	Sample	THM
2) 684.45	2) 740.00	2) 802.88
342.22	370.00	401.44

Temperature Drops

BHM: 11.83

Sample: 44.00

THM: 12.60

k Heat Meters, watts / m deg C

BHM: 3.29 @ 342 °C

THM: 3.22 @ 401 °C

$$k_s = k_{HM} \left[\frac{\Delta T_{HM}}{\Delta T_s}\right] \left[\frac{X_s}{X_{HM}}\right]$$

$k_s \Big|_{BHM} = 3.29 \times \frac{11.83}{44.00} \times \frac{1.589}{1.198} = 1.17$

$k_s \Big|_{THM} = 3.22 \times \frac{12.60}{44.00} \times \frac{1.589}{1.198} = 1.22$

Energy Spread

$$\frac{k_s \Big|_{BHM} - k_s \Big|_{THM}}{k_s \Big|_{BHM} + k_s \Big|_{THM}} \times 100 = 4\ \%$$

2) 2.39

$k_s = 1.20$ watts / m deg C @ 370 °C

By: AOD

Date: 9 Dec 76

05-05-10/74

DYNATECH CORPORATION — THERMAL CONDUCTIVITY DATA SHEET

Project: NAS-39-1 Test Method: Comp Temperature Point: 390 C

Environment: Argon / Center T/C Material: K Date: 8 Dec 75

Coolant: H_2O Guard: API Aux. Htr: API Sink Ins.: IBP

Sample: Number: ETC-3 Description: $LiOH$ Reagent

Sample Geometry: Standard

		Gross Δx	T/C	Net Δx	
Top					
Bottom					

Time	925	925	1000				
T/C 1	13.719	13.719	13.719				
2	14.213	14.214	14.214				
3	14.208	14.208	14.208				
4	16.058	16.059	16.058				
5	16.190	16.191	16.190				
6	16.722	16.722	16.721				
7	15.255	15.254	15.254				
8							
9							
10							
11							
12						M ⇒	995 L
						G ⇒	831 L
						A ⇒	760 L
Main Htr. Voltage	←		→				
Main Htr. Current							
Main Htr. Power							
ΔT top HM	532	531	531				
ΔT bottom HM	495	495	495				
ΣΔT HM	1.027	1.026	1.026				
ΔT≤	1.850	1.851	1.850				
T							
Index	.555	.554	.555				
Pressure							
Operator							

Additional Information:

MELTING POINT (±3°C) 252.7C 447 J/g 5.33 × 10⁵ J/Kg

HEAT OF FUSION = ~~[illegible]~~ 122.1 × 60 = 8280 J × .535 W = 4430 J / .00831 Kg =

DYNATECH CORPORATION QTA DATA REDUCTION

Date: 2/14/76 Data of: 2/10/76 Project: NAS-58-1

Sample: $LiNO_3$ Reagent Weight before: .00879 kg: after: .00783 kg: (.00831 mean)

Power: .535 watts x 60 sec/min = 32.1 watt - sec/min

V mv	T °C	dV/dt mv/min	dV/dT mv/deg C	dT/dt deg C/min	q watt-sec/min	mc_p of s + c joule/deg C	$mc_{p(c)}$ joule/deg C	$mc_{p(s)}$ joule/deg C	$c_{p(s)}$ joule/kg deg C
-5.25	-182.5		0.01769						
-5.00	-169.1		0.01962						
-4.75	-156.8		0.02115						
-4.50	-145.4		0.02255						
-4.00	-124.4		0.02525						
-3.50	-105.4		0.0276						
-3.00	- 87.9		0.02955						
-2.50	- 71.4		0.03135						
-2.00	- 55.9		0.0330						
-1.50	- 41.1		0.03445						
-1.00	- 26.9		0.03595						
-0.50	- 13.2		0.03725						
0	0		0.0385						
0.50	12.8		0.03965						
1.00	25.3	.0435	0.0408	1.066	32.1	30.11	12.93	12.18	1386
1.50	37.4	.0449	0.0417	1.077	"	29.80	18.09	11.71	1332
2.00	49.2	.0459	0.04275	1.074	"	29.89	18.44	11.45	1303
2.50	60.8	.0455	0.0437	1.041	"	30.84	18.85	11.99	1364
3.00	72.1	.0459	0.0446	1.029	"	31.20	19.30	11.90	1354
3.50	83.2	.0463	0.04545	1.019	"	31.50	19.65	11.85	1348
4.00	94.0	.0460	0.0462	.996	"	32.23	19.75	12.48	1420
4.50	104.7	.0461	0.0470	.981	"	32.72	20.02	12.70	1445
5.00	115.3	.0460	0.0479	.960	"	33.44	20.35	13.09	1489
5.50	125.6	.0461	0.04855	.950	"	33.79	20.90	12.89	1466
6.00	135.9	.0460	0.0493	.933	"	34.41	21.04	13.37	1521
6.50	145.9	.0458	0.0499	.918	"	34.97	21.23	13.74	1563
7.00	155.9	.0460	0.0506	.909	"	35.31	21.60	13.71	1560
7.50	165.7	.0461	0.0512	.900	"	35.67	21.86	13.81	1571
8.00	175.4	.0461	0.0518	.890	"	36.07	22.04	14.03	1596
8.50	185.1	.0461	0.0523	.881	"	36.44	22.25	14.19	1614

DYNATECH CORPORATION QTA DATA REDUCTION

Date: 2/14/76 Data of: 2/10/76 Project: NAS-52-1

Sample: $LiNO_3$ Weight before: .00879 kg. after: .00783 kg.

Power: .535 watts × 60 sec/min = 32.1 watt - sec/min

V mv	T °C	$\frac{dV}{dt}$ $\frac{mv}{min}$	$\frac{dV}{dT}$ $\frac{mv}{degC}$	$\frac{dT}{dt}$ $\frac{deg\ C}{min}$	q $\frac{watt\ s}{min}$	mc of p S+C $\frac{joule}{degC}$	$mc_{p(c)}$ $\frac{joule}{deg\ C}$	$mc_{p(s)}$ $\frac{joule}{deg\ C}$	$c_{p(s)}$ $\frac{joule}{kg\ deg\ C}$
9.0	194.6	.0460	0.0529	.870	32.1	36.90	22.57	14.33	1630
9.5	204.0	.0460	0.0534	.861	"	37.28	22.79	14.49	1648
10.0	213.3	.0460	0.0539	.853	"	37.63	23.08	14.55	1655
10.5	222.5	.0450	0.0544	.827	"	38.81	23.35	15.46	1759
11.0	231.7	.0440	0.0549	.851	"	40.07	23.62	16.45	1871
11.5	240.7	.0428	0.0553	.774	"	41.47	23.80	17.67	2010
12.0	249.7	.0255	0.0558	.457	"	70.24	24.08	46.16	5555
12.5	258.7	.0438	0.0562	.780	"	41.15	24.30	16.85	2151
13.0	267.5	.0450	0.0566	.795	"	40.38	24.33	16.05	2050
13.5	276.3	.0440	0.0570	.772	"	41.58	24.67	16.91	2160
14.0	285.1	.0436	0.05745	.762	"	42.13	24.86	17.27	2207
14.5	293.7	.0434	0.0578	.751	"	42.74	25.21	17.53	2239
15.0	302.2		0.0582						
15.5	310.9		0.0586						
16.0	319.4		0.0589						
16.5	327.9		0.0592						
17.0	336.3		0.0596						
17.5	344.7		0.0600						
18.0	353.0		0.0603						
18.5	361.2		0.0607						
19.0	369.5		0.0613						
20.0	385.8		0.0617						
20.5	393.9		0.0620						

SAMPLE # 2 $LiOH = 29.71g$ **DROP CALORIMETER** **PROJECT:** NAS-58-1

Cont #2 = 83.945g Tot wt 113.66g **DATE:** 12/30/75

TIME	DIFF.	OIL	WATER	SAMP.
11:05	+.190	.740	.724	13.618
:22	.188	.741	.725	13.566
12:55	.186	.744	.728	13.877
:57	.186	.744	.728	13.877
:58	.186	744	.728 ↓	13.875
13:00	.324			Drop
:01	.379			
:02	.431			
:05	.557			
:07	.622			
:10	.699			
:12	.740			
:25	.892			
:36	.940			
:51	.963			
:52	.963			
:53	.964			
14:07	.964			
:20	.959			
:30	.952			
:37	.945			
:55	.929			
17:38	.831			

23 volts

TS 1 340.02 $\Delta T = 319.69$

S 2

R 1 18.25

R 2 20.3317

ΔT DIFF. $\frac{.836}{.4016} = 2.081$

$\frac{17791 \times 2.0817}{319.69}$

Using 19,240 J/°C as MC, R for 340°C drop:

$19,240 \times 2.0817 = 40,052$ J Tot

$-13,851$ J/cont $= 26,200$ J/Samp

$\div .02971$ kg $= 881,874$ J/kg

$\div 319.69$°C $= 2758$ J/kg °C

or .6589 cal/g °C

325,845 J/kg Tot

161,000 J/kg cont

164,845 J/kg Samp

46 1510

NAS-5E-1

MV

1022

1.050
1.000
.950
.900
.850
.800
.750
.700
.650
.600
.550
.500
.450
.400
.350
.300
.250
.200
.150

B6

0 10 20 30 40 50 60 120 180

Time (min)

13 21 1226

JARRELL-ASH DIVISION
Fisher Scientific Company

Certificate of Analysis

TO: Dynatech R/D Company
99 Erie Street
Cambridge, MA 02139
Attn: Mr. A. Desjarlais

DATE RECEIVED: 8/2/76
DATE REPORTED: 8/6/76
ORDER NO.: 13597

SAMPLE DESCRIPTION: $LiNO_3$
INSTRUMENTATION: 3.4 Meter Ebert Mark IV Spectrograph

	1	2			1	2			1	2			1	2	
Li	H	H		Zn	ND	ND		Sb	ND	ND		Lu			
Be	ND	ND		Ga	ND	ND		Te	ND	ND		Hf	ND	ND	
B	ND	10		Ge	ND	ND		Cs	ND	ND		Ta	ND	ND	
Na	5	400		As	ND	ND		Ba	ND	5		W	ND	ND	
Mg	5	100		Rb	ND	ND		La				Re	ND	ND	
Al	.1	400		Sr	ND	ND		Ce				Os	ND	ND	
Si	1	>.1%		Y				Pr				Ir	ND	ND	
K	ND	ND		Zr	ND	ND		Nd				Pt	ND	ND	
Ca	300	800		Nb	ND	ND		Sn.				Au	ND	ND	
Ti	ND	50		Mo	ND	ND		Eu				Hg	ND	ND	
V	ND	1		Ru	ND	ND		Gd				Tl	ND	ND	
Cr	ND	10		Rh	ND	ND		Tb				Pb	ND	ND	
Mn	.5	2		Pd	ND	ND		Dy				Bi	ND	ND	
Fe	1	100		Ag	ND	ND		Ho				Th			
Co	200	500		Cd	ND	ND		Er				U			
Ni	10	5		In	ND	ND		Tm				P	ND	ND	
Cu	.1	20		Sn	ND	ND		Yb				Se			

REMARKS: 1 = Reagent; 2 = Commercial; Results in ppm except where percent is indicated.

KEY:

ND - Not Detected		T	.01 -.1%
VVFT	< .0001%	L	.1- 1%
VFT	.0001% - .001%	M	1% -10%
FT	.001% - .01%	H	>10%

STAFF ANALYST

SUPERVISOR, TESTING LABS

JARRELL-ASH DIVISION
Fisher Scientific Company

Certificate of Analysis

TO: Dynatech R/D Company
99 Erie Street
Cambridge, MA 02139
Attn: Mr. A. Desjarlais

DATE RECEIVED. 8/2/76
DATE REPORTED: 8/6/76
ORDER NO.: 13597

SAMPLE DESCRIPTION: Li Cl/Li OH Eutectic
INSTRUMENTATION. 3.4 Meter Ebert Mark IV Spectrograph

	5	6			5	6			5	6			5	6	
U	H	H		Zn	ND	ND		Sb	ND	ND		Lu			
Be	ND	ND		Ga	ND	ND		Te	ND	ND		Hf	ND	ND	
B	ND	5		Ge	ND	ND		Cs	ND	ND		Ta	ND	ND	
Na	25	1000		As	ND	ND		Ba	5	5		W	ND	ND	
Mg	1	100		Rb	ND	ND		La				Re	ND	ND	
Al	.5	500		Sr	ND	ND		Ce				Os	ND	ND	
Si	100	>.1%		Y				Pr				Ir	ND	ND	
K	ND	ND		Zr	ND	ND		Nd				Pt	ND	ND	
Ca	100	200		Nb	ND	ND		Sn.				Au	ND	ND	
Ti	ND	50		Mo	ND	ND		Eu				Hg	ND	ND	
V	ND	1		Ru	ND	ND		Gd				Tl	ND	ND	
Cr	ND	500		Rh	ND	ND		Tb				Pb	ND	ND	
Mn	.1	1		Pd	ND	ND		Dy				Bi	ND	ND	
Fe	1	100		Ag	ND	ND		Ho				Th			
Co	200	500		Cd	ND	ND		Er				U			
Ni	5	500		In	ND	ND		Tm				P	ND	ND	
Cu	1	10		Sn	ND	ND		Yb				Se			

REMARKS: 5 = Reagent; 6 = Commercial; Results in ppm except where percent is indicated.

KEY:			
ND - Not Detected		T	.01 -.1%
VVFT	< .0001%	L	.1- 1%
VFT	.0001% - .001%	M	1% -10%
FT	.001% - .01%	H	>10%

STAFF ANALYST

SUPERVISOR, TESTING LABS

JARRELL-ASH DIVISION
Fisher Scientific Company

Certificate of Analysis

TO: Dynatech R/D Company
99 Erie Street
Cambridge, MA 02139
Attn: Mr. A. Desjarlais

DATE RECEIVED: 8/2/76
DATE REPORTED: 8/6/76
ORDER NO.: 13597

SAMPLE DESCRIPTION: Li OH

INSTRUMENTATION: 3.4 Meter Ebert Mark IV Spectrograph

	3	4			3	4			3	4			3	4	
Li	H	H		Zn	ND	ND		Sb	ND	ND		Lu			
Be	ND	ND		Ga	ND	ND		Te	ND	ND		Hf	ND	ND	
B	ND	ND		Ge	ND	ND		Cs	ND	ND		Ta	ND	ND	
Na	ND	ND		As	ND	ND		Ba	ND	ND		W	ND	ND	
Mg	.5	.1		Rb	ND	ND		La				Re	ND	ND	
Al	.5	.5		Sr	ND	ND		Ce				Os	ND	ND	
Si	100	80		Y				Pr				Ir	ND	ND	
K	ND	ND		Zr	ND	ND		Nd				Pt	ND	ND	
Ca	50	20		Nb	ND	ND		Sm				Au	ND	ND	
Ti	ND	ND		Mo	ND	ND		Eu				Hg	ND	ND	
V	ND	ND		Ru	ND	ND		Gd				Tl	ND	ND	
Cr	ND	10		Rh	ND	ND		Tb				Pb	ND	ND	
Mn	.5	.1		Pd	ND	ND		Dy				Bi	ND	ND	
Fe	20	40		Ag	ND	ND		Ho				Th			
Co	200	50		Cd	ND	ND		Er				U			
Ni	ND	ND		In	ND	ND		Tm				P	ND	ND	
Cu	ND	ND		Sn	ND	ND		Yb				Se			

REMARKS: 3 = Reagent; 4 = Commercial; Results in ppm.

KEY:			
ND - Not Detected		T	.01 -.1%
VVFT	< .0001%	L	.1- 1%
VFT	.0001% - .001%	M	1% -10%
FT	.001% - .01%	H	>10%

STAFF ANALYST

SUPERVISOR, TESTING LABS

JARRELL-ASH DIVISION
Fisher Scientific Company

Certificate of Analysis

TO: Dynatech R/D Company
99 Erie Street
Cambridge, MA 02139
Attn: Mr. A. Desjarlais

DATE RECEIVED. 8/2/76
DATE REPORTED. 8/6/76
ORDER NO.: 13597

SAMPLE DESCRIPTION: $Na_2 B_4 O_7$ Reagent
INSTRUMENTATION: 3.4 Meter Ebert Mark IV Spectrograph

Li	ND			Zn	ND			Sb	ND			Lu			
Be	ND			Ga	.5			Te	ND			Hf	ND		
B	H			Ge	ND			Cs	ND			Ta	ND		
Na	H			As	ND			Ba	ND			W	ND		
Mg	2			Rb	ND			La				Re	ND		
Al	10			Sr	ND			Ce				Os	ND		
Si	100			Y				Pr				Ir	ND		
K	ND			Zr	ND			Nd				Pt	ND		
Ca	1			Nb	ND			Sm				Au	ND		
Ti	ND			Mo	ND			Eu				Hg	ND		
V	ND			Ru	ND			Gd				Tl	ND		
Cr	75			Rh	ND			Tb				Pb	ND		
Mn	25			Pd	ND			Dy				Bi	1		
Fe	800			Ag	250			Ho				Th			
Co	ND			Cd	ND			Er				U			
Ni	ND			In	ND			Tm				P	ND		
Cu	2			Sn	ND			Yb				Se			

REMARKS: Results in ppm except when percent is indicated.

KEY:

ND - Not Detected		T	.01 - .1%
VVFT	< .0001%	L	.1 - 1%
VFT	.0001% - .001%	M	1% - 10%
FT	.001% - .01%	H	>10%

STAFF ANALYST

SUPERVISOR, TESTING LABS